NASA Technical Memorandum 88336

Aerodynamic Characteristics of the Modified 40- by 80-Foot Wind Tunnel as Measured in a 1/50th-Scale Model

Brian E. Smith and Tim Naumowicz

August 1987

NASA

National Aeronautics and
Space Administration

Aerodynamic Characteristics of the Modified 40- by 80-Foot Wind Tunnel as Measured in a 1/50th-Scale Model

Brian E. Smith, Ames Research Center, Moffett Field, California
Tim Naumowicz, Robinson Engineering, San Carlos, California

August 1987

SUMMARY

The aerodynamic characteristics of the 40- by 80-Foot Wind Tunnel at Ames Research Center were measured by using a 1/50th-scale model of the full-scale facility. The model was configured to closely simulate the features of the full-scale facility when it becomes operational in 1986. The items measured include the aerodynamic effects due to changes in the total-pressure-loss characteristics of the intake and exhaust openings of the air-exchange system, total-pressure distributions in the flow field at locations around the wind tunnel circuit, the locations of the maximum total-pressure contours, and the aerodynamic changes caused by the installation of the acoustic barrier in the southwest corner of the wind tunnel. The model tests reveal the changes in the aerodynamic performance of the 1986 version of the 40- by 80-Foot Wind Tunnel compared with the performance of the 1982 configuration.

INTRODUCTION

As part of the aerodynamic verification testing of the National Full-Scale Aerodynamics Complex (NFAC) modification, a test of the 40- by 80-Foot Wind Tunnel was performed using a 1/50th-scale model of the tunnel. The model was configured to closely simulate the changes made to the facility since the 1982 Integrated Systems Test (IST). The objective of the tests was to determine the aerodynamic characteristics of the facility as it will exist when it becomes operational in 1986. A planview of the NFAC is shown in figure 1.

The 1/50th-scale model (fig. 2) has been used extensively for aerodynamic studies of the NFAC in both the closed-circuit and open-return modes of operation (ref. 1). In particular, the model has been used to test various concepts for the new air-exchange inlet, shown in figure 3. Recent tests (refs. 2 and 3) focused on the effects of the new inlet design on the airstream characteristics downstream of the intake door and on the air-exchange rate. During these tests, no attempt was made to simulate the screen on the air-exchange inlet which will be necessary in the full-scale facility to prevent the entry of unwanted debris.

In the present series of tests, the debris screen and its associated supporting super-structure, which are proposed for the courtyard air-exchange inlet of the full-scale facility, was simulated by a 30-mesh screen, and a wood and sheet-metal model of the superstructure (fig. 4). In addition, the west column of louvers at the air-exchange exhaust, located at the southwest corner of the facility, was changed from a configuration in which only three or five louvers were open to a fully open configuration. Figure 5 shows the two panels used to simulate these configurations. The full-open panel is shown installed in the

south end of the model. The five-door panel is shown on the right of the figure. These modifications were expected to produce changes in the air-exchange rate for a given door opening, and to change the differential wall pressures in the north and south legs of the facility. The modifications were also expected to affect the dynamic-pressure distribution across the test section. In addition to the modifications made to the air-exchange system, the airfoil contour of the primary diffuser support struts was also changed. This modification was necessary because the existing struts were not representative of the struts in the full-scale diffuser. The vortex generators proposed for the primary diffuser were also installed in the model.

The increased open area of the air-exchange exhaust was estimated to increase the noise radiated to the community when powered models are tested (Soderman, P.: Investigation of the Community Noise Footprint Due to a Source in the Test Section of the 40- by 80-Foot Wind Tunnel at Ames Research Center. Private communication.). To reduce the noise level, an acoustic barrier was proposed for installation in the southwest corner of the wind tunnel. A final series of model tests were therefore performed to determine the aerodynamic effects brought about by the acoustic barrier.

TEST FACILITY

The wind tunnel used for these tests is a 1/50th-scale model of the NFAC 40- by 80-Foot Wind Tunnel. The overall dimensions of the model are approximately 18 ft long, 9 ft wide, and 3 ft high. The test section has an oval cross section that has internal dimensions of 0.66 ft high by 1.33 ft wide. The maximum velocity in the test section is approximately 240 ft/sec, which corresponds to a dynamic pressure of 65 lb/ft^2. Other than fan speed, the only other variable in the operation of the model tunnel is the position of the air-exchange inlet door. The door was built so that it could be set at any position from closed to an open position equal to 10% of the width of the corridor at the north leg.

The acoustic lining in the test section is simulated in the model by a layer of plastic 0.125 in. thick. As in the full-scale facility, the upstream side of the acoustic liner is faired onto the tunnel surface by a 3:1 ramp. The downstream end of the liner is also faired onto the surface of the primary diffuser by a 3:1 ramp. In the full-scale facility, this ramp will have a 10:1 slope.

The primary diffuser downstream of the test section incorporates the vortex-generator design planned for the full-scale wind tunnel. The location and configuration of the vortex generators are shown in figure 6. The vortex generators are identical in planform and location to the full-scale design, but they were represented in the model with flat sheet-metal

2

plates instead of the airfoil section of the full-scale versions. The vortex generators are intended to prevent surging of the flow in the wind tunnel.

The primary diffuser also contains the ceiling support struts of the full-scale tunnel. The column protection device at the base of the first strut is simulated as is the model-catcher screen located on the floor at the downstream end of the diffuser. The airfoil contour of the struts was changed to the actual airfoil shape of the full-scale struts (fig. 7) because the faired cylinder shape of the original struts in the model was possibly creating an excessively wide wake in the center of the diffuser. This wake was thought to create regions of high dynamic pressure on both sides of the diffuser caused by the effective blockage of the flow by the wake of the support struts.

The model is powered by six three-phase, induction-type electric motors with variable-frequency power for variable-speed operation. The motors are water-cooled, and the rated power for each motor is 10 hp at 10,000 rpm. The maximum speed achieved in the present investigation was 6,500 rpm. Each motor drives a six-bladed, fixed-pitch fan with a diameter of 9.5 in. and with a hub diameter of 4.2 in. A single row of stator blades is located downstream of the blade disk in each fan duct. The sense of rotation of the fans is opposite to that of the motors in the full-scale wind tunnel.

With the exception of vane set 5, all of the turning vanes have the proper scale and airfoil contour. Vane set 5 is identical in configuration to the original design of vane set 5, which incorporated flat-plate airfoils with a deflected leading edge. Because of the time and expense required to build a scale model of the new, nonmoving vane set, it was decided that the original design was adequate for the present investigation of the 40- by 80-Foot wind tunnel circuit.

Unique Features of Instrumentation

The collection of pressure data during tests of the 1/50th-scale model of the 40 by 80 was greatly facilitated by use of electronically scanned pressure-measurement instrumentation. The pressure-measurement system utilized in the tests is a fully integrated test instrument which uses a transducer at each measurement port. The technique behind electronic pressure scanning consists of utilizing low-cost, silicon pressure transducers in which inherent errors (linearity, thermal zero shift, and output drift with time) are corrected by periodic on-line calibrations using a highly accurate secondary standard.

The system has the capability to measure up to 1024 pressures at data rates of up to 20,000 measurements/sec with inaccuracies of no more than ±0.1% of full scale. The high system accuracy is derived from an internal, quartz reference transducer which corrects for all thermal and sensitivity shifts, including nonlinearity of the transducers, the amplifiers, and the analog-to-digital converter. During the tests, the system was controlled by an on-line minicomputer, which was also used for subsequent data reduction and display. The

high data rates offered by the system enabled 88 static pressures around the circuit to be sampled simultaneously. The system also permitted the pressures to be averaged over a user-specified time period.

Total pressures in the flow field were measured at seven cross-stream stations around the circuit. Pressures were measured at eight vertical locations using an eight-probe rake which was traversed horizontally across the tunnel. The data allowed total-pressure contours to be generated at each station. The rake-traversing mechanism and the pressure-measurement system were controlled by the minicomputer. At each lateral position of the rake, static pressure measurements were made which allowed computation of the test-section dynamic pressure, and verification of the pressure rise across each of the tunnel fan-drive units. Test-section total-pressure traverses were made with a single Kiehl probe.

The air-exchange rate was determined by the use of an air-conditioning-type balometer. This device measures the airflow past a calibrated grid of total and static pressure orifices. The balometer was used to measure the volume rate of flow through the air-exchange intake.

Calibration of Static-Ring Dynamic Pressure for Test Section

To obtain a nonintrusive measurement of test-section dynamic pressure, measurements of the static pressure immediately upstream and downstream of the contraction to the test-section were made. The same technique is used to measure test section dynamic pressure in the full-scale 40 by 80. In the full-scale facility, static pressure taps are located at each end of the bell-mouth contraction leading to the test section. The taps are positioned on the side walls and on the ceiling. The static pressures measured at the upstream end of the contraction are mechanically averaged by connecting them to a common manifold, the static ring. The same averaging technique is used for the static pressures measured at the downstream or test section end of the contraction. In the model, these pressure measurements were calibrated against a pitot-static probe mounted on the centerline of the test section. Because of the possibility of leak-induced errors in the measurement of the mechanically averaged pressures, and because of the possibilities of surface irregularities near the static-pressure orifices, various combinations of the static orifices at each end of the contraction were evaluated to determine which set of orifices produced the best agreement with the pressures measured by the pitot-static probe. As a result of this experimentation, it was found that three, ganged, static ports upstream of the contraction, and a single static port in the test section yielded the best agreement with the pitot-static probe in the test section. Figure 8 shows how these taps were connected. The accuracy of the pitot-static measurement in the test section was limited to the reading accuracy of the water manometer to which the probe was connected. A linear-regression technique was used to obtain an equation for the conversion of the static-ring pressures to the actual test-section dynamic pressure. Figure 9 is a plot of the difference between

4

the pitot-static differential pressure and the static-ring differential pressure as a function of the static-ring dynamic pressure measurement.

Measurement of Air-Exchange Rate

The debris screen and associated supporting superstructure proposed for the court-yard air-exchange inlet of the full-scale facility was simulated by a 30-mesh screen and a model of the superstructure. Also, the west column of louvers at the south-end, air-exchange exhaust was changed to a fully open arrangement with the vanes of vane set 7 in the open position. A debris screen was also simulated at the exhaust opening. The air exchanger is a passive system wherein neither the inlet nor the exhaust is driven (i.e., pumped). The flow rate through the inlet and exhaust openings is therefore determined by the sizes of the openings, the total-pressure-loss characteristics of the screen, and the pressure difference between the inside of the tunnel and the atmosphere. The modifications to the model change the total-pressure-loss characteristics of the intake and exhaust openings from the configuration of reference 2, thereby altering the mass rate of flow through these openings. The calculated total-pressure-loss coefficient of the debris screen used in the model is 0.431. The loss coefficient is defined as the drop in total pressure across the screen divided by the onset dynamic pressure. The loss coefficient is related to the percentage of open area of the screen by the formula, $k = 0.52 \frac{(1-\beta^2)}{\beta^2}$. The loss coefficient of the screen used in the model tests compares favorably with the calculated loss coefficient of 0.432 for the debris screen proposed for the full-scale facility. In addition to simulating the loss of the debris screen, the loss of the superstructure was also simulated. The loss characteristics of the full-scale superstructure was simulated in the model by adjusting the size and spacing of the framework members (fig. 4) to obtain a loss estimated for the full-scale device.

The initial phase of the aerodynamic testing involved the measurement of the air-exchange rate as a function of inlet door position and test-section dynamic pressure. The volume rate of flow through the air-exchange inlet was measured with an Alnor balom. This device measures airflow by mechanically integrating the total versus static pressure differential across a known area and then converting the pressure difference to cubic feet per minute through a calibrated meter. The device is accurate to ±3% of full scale. The test-section mass rate of flow was calculated from the measured dynamic pressure and the test-section cross-sectional area.

Figure 10 is a plot of the air-exchange rate as a function of the opening of the air-exchange door in percentage of the width of the north-end channel. The closed symbols represent data taken during the 1982 IST (ref. 2). The remaining curves, denoted with open symbols, represent data taken with the 1/50th-scale model. The 1/50th-scale curves show the effect on air exchange as a result of the various configurations tested with the model. For both the five-panels-removed case and the west-column-of-doors-open case,

5

the simulated debris screen and its associated support structure had the effect of slightly reducing the flow through the air-exchange inlet.

Figure 11 is a plot of the change in air-exchange rate with increases in the dynamic pressure test section. Each set of four curves represents data taken with either the west column configured with five doors open or with the west column fully open. Within each set of curves, four different door-opening percentages are shown. Increasing the test-section dynamic pressure causes a slight reduction in the measured air-exchange rate for both exhaust configurations.

Measurement of Differential Wall Pressure

Static pressures referenced to atmospheric pressure were measured simultaneously at 88 locations on the model using the electronic-scanning, pressure-measurement instrumentation. Figure 12 shows the locations around the model from which the measurements were made. Thirty samples were averaged over a period of approximately 0.1 sec for each data point. The differential pressures were measured for four different levels of test-section dynamic pressure and three settings of the air-exchange inlet-door position. The pressure data were taken with the five-door west-column configuration and with the fully open west column. The pressures have been nondimensionalized by dividing by the calculated test-section dynamic pressure. The static ring pressures used to compute the dynamic pressure were measured at the same time as were the circuit pressures. Figures 13 and 14 show the variation of the differential wall-pressure coefficient along the centerline of the model for the two exhaust configurations. The plot starts at the beginning of the constant-area section upstream of the contraction to the test section. The labels across the top of the figures indicate the major sections of the circuit. The four curves on each figure represent data taken at four successively higher test section dynamic pressures with the air-exchange inlet door set at the 50% open position. The increased open area of the fully open exhaust configuration decreases the pressure coefficient throughout the circuit by approximately 0.07.

Figures 15-18 illustrate the change in differential wall-pressure coefficient with various air-exchange rates. The ratio of the smallest to the largest dynamic pressures for these cases is approximately 1:4. This corresponds to an approximate doubling in test-section velocity. The three curves on each of the plots represent three successively greater air-exchange rates. These plots were generated with data taken with the west column in the fully open configuration. The principal effect of increasing the tunnel velocity is a slight increase in pressure across the north corridor of the model. The cause of this phenomenon is uncertain.

Figure 19 shows the maximum full-scale differential-wall-pressure variation predicted in pounds per square foot. The pressures were calculated by multiplying the pressure coefficient measured on the model by the maximum anticipated test section dynamic pressure

6

in the full-scale facility, 262 lb/ft^2. Also shown on the figure are results from the 1982 IST. The test-section dynamic pressure for these data is 274 lb/ft^2. The air-exhaust configuration for the 1982 IST was a three-door-open configuration. According to this comparison, the fully open exhaust configuration results in approximately a 20 lb/ft^2 increase in pressure throughout the circuit.

Because a large number of static pressure measurements were made around the model, it was possible to compare the pressures at certain cross-stream stations. Figures 20-22 show the variation in static pressure among the taps located at seven stations around the circuit. The three curves on each figure represent different air-exchange rates. The diagrams on the figures show the locations at which the comparisons were made and the system used for representing the static pressures at a given station. When looking downstream, the pressure taps are located at 0, 90, 180, and 270° from the courtyard sidewall.

Plots were made of the change in static pressure along the north and south end outside walls. Figures 23a and b show the variation in the pressure coefficients along the north and south walls. The three curves on each graph represent data from different air-exchange rates. The diagram on the figure shows the locations of the pressure taps along each wall and the x-coordinate system location for each plot. Figures 24a and b show the variation in north- and south-leg pressure coefficients versus air-exchange rate for two pressure taps located as shown on the diagram. The four curves represent different levels of test-section dynamic pressure.

An attempt was made to calculate the pressure-loss coefficients of vane sets 1, 2, 6, and 8. This was a proof-of-concept experiment for the 40 by 80 IST. It was theorized that the loss coefficients of a vane set could be estimated by plotting the static pressure change as a function of streamwise distance on either side of a particular vane set. A linear regression techinque was used to fit a line through the data points on each side of the vane set. At the location of the vane set, a pressure jump was expected to be observed between the two lines. The pressure-loss coefficient is calculated by dividing this pressure jump by the local dynamic pressure at the vane set. Figure 25a shows how the pressure jumps were estimated for vane sets 1 and 2. The vane set 1 loss coefficient is estimated to be approximately 0.09 at 5% air exchange, and the loss coefficient for vane set 2 is estimated to be approximately 0.23. Estimating the loss coefficients of vane sets 6 and 8 required pushing the instrumentation to the limit of its resolution because of the low differential pressure between tunnel static pressure at the south end and atmospheric pressure. An average of 60 samples over a time period of 1 sec was used for each data point. Figure 25b shows the static pressure variation on either side of vane sets 6 and 8 for 5% air exchange. From this figure, the loss coefficients of vane sets 6 and 8 are estimated to be approximately 0.77 and 0.03, respectively.

Cross-Stream Dynamic Pressure Contours

Total-pressure flow-field surveys were made at various locations in the 1/50th-scale 40- by 80-Foot wind tunnel model. In the test section, the surveys were made along the horizontal centerline of the test section. The survey line was located at the streamwise midpoint of the test section. A Kiehl probe was used to obtain total pressure. During each traverse, the static pressure at the top of the test section was measured at the location shown in figure 8. This local static pressure was subtracted from the total pressure measured by the traversing probe and then divided by the actual test section dynamic pressure to obtain a total pressure coefficient. Figure 26a shows the variation in this coefficient across the test section for three different air-exchange rates. The west side of the circuit is to the left in the figure and the courtyard side is to the right. The dynamic pressure in the test section during these runs was approximately 25 lb/ft^2. The variation among the curves at the left side of the graph is due to the recirculation region which occurs downstream of the air-exhaust opening. The shape and size of this region of recirculating flow changes depending upon the air-exchange rate. The total pressure deficit resulting from this condition persists through vane set 8 and can be measured in the test section. Figure 26b shows the lateral variation in the pressure coefficient for a test-section dynamic pressure of approximately 60 lb/ft^2.

Total-pressure-coefficient contours were computed from rake surveys done at various locations around the circuit. Figures 27a and b show the total-pressure contours looking upstream at the end of the primary diffuser for air-exchange rates of 5.9 and 10.1% , respectively. The wake from the diffuser ceiling-support struts is visible near the upper center of the plot. Two kidney-shaped regions of high-energy core flow are evident to the right and left of lower center. The horizontal rows of dots represent the locations where the total pressure data were taken.

Figures 28a and b show the dynamic pressure contours 1 in. downstream of the air-inlet door for air-exchange rates of 5.9 and 10.1% , respectively. The arrows at the top and bottom of each figure represent the relative location of the trailing edge of the air-exchange inlet door. The wake from the inlet door and the high-velocity air from the inlet are evident at the right side of the plots. The wake from the diffuser struts and the regions of high-velocity flow seen at the end of the primary diffuser are still present. Figures 29a and b show contours generated from data taken during narrow surveys immediately downstream of the inlet door. The width of the surveys was equal to twice the door opening. Again, the wake of the door and the high-velocity air from the air-exchange inlet are visible to the right. The injection of cooling air boosts the total-pressure coefficients near the wall to a value more nearly equal to the centerline values shown in figure 28.

Figures 30a and b compare the courtyard-wall dynamic-pressure profiles 1 in. downstream of the inlet door and 1 in. or two chords behind vane set 2 for 5 and 10% air-exchange rates. The data are taken from the fifth survey line from the bottom shown

on figures 28a and b. Distances are shown scaled to the full-scale facility. The location of the trailing edge of the inlet door is shown to scale on each figure. Immediately downstream of the intake door, a wall jet of high-velocity air exists which is approximately as wide as the door opening. After passing through vane set 2, the peak total-pressure values in this jet decrease by approximately 25% , and the jet spreads in width by about 30% . This jet pumps energy into the boundary layer on the courtyard wall and should decrese the apparent thickness of the boundary layer entering fans 1 and 4. The result of this will be a reduction in the oscillatory loading caused by fan inflow assymetry which was recorded during the 1982 IST.

Figures 31a and b show the total-pressure contours at the end of the fan drive diffuser for 5.9 and 10.1% air exchange, respectively. The total-pressure field at this location is clearly very disorganized. This is due to residual swirl from the fans and the resulting mixing of the flow. Figures 32a, b, and c show the total-pressure contours midway between vane sets 6 and 8 for air-exchange rates of 0, 5.9, and 10.1% , respectively. At the 10.1% air-exchange condition, the average total pressure in the flow adjacent to the outside wall is higher than in the 0 and 5.9% cases. As a greater percentage of air is allowed to flow through the exhaust opening, the effective area downstream of vane set 6 increases because a reduced amount of air flows through the south corridor. This has the effect of pulling the flow toward the side of the circuit where the exhaust opening is located. In addition, the total-pressure level in the flow on the courtyard side of the south corridor is substantially less than on the outside of the circuit. This may be due to underturning of the flow by vane set 6.

Acoustic-Barrier Aerodynamic Studies

During operation of the wind tunnel at high test-section velocities, the pressure in the south end of the facility can exceed structural limits. To prevent this from happening, the louvers of the west column of vane set 7 will be fixed in an open position. The west column of vane set 7 forms the air-exhange system exhaust opening (fig. 33). Since these louvers will be permanently open, noise from powered models in the test section can radiate into the community. Measurements of the sound-pressure levels in the community caused by a noise source in the test section indicate a potential noise problem. To prevent this from occurring, an acoustic barrier to the noise path was proposed. As shown in figure 34, this barrier is formed by a wall connecting the trailing edge of vane 51 of vane set 6 to the south wall of the wind tunnel. The wall extends from floor to ceiling. The wall is approximately 20 ft wide and 130 ft high. With the barrier in this position, the sound from a powered model in the test section is effectively prevented from radiating into the community.

The acoustic barrier has several effects on the aerodynamics of the wind tunnel. The wall changes the location where the south end of the circuit is vented to atmospheric

pressure. With the wall in place as shown on figure 34, the region upstream of vane set 6 is vented to atmospheric pressure. If the wall is removed, the region of the circuit downstream of vane set 6 would be vented to the atmosphere. A change in the location of this venting can affect the performance of the air-exchange system. It can also affect the pressure balance between the north and south ends of the wind tunnel, as well as the differential pressures across the walls of the south end.

The acoustic barrier also changes the aerodynamics of the southwest corner of the circuit. In order to install the wall, three of the trailing-edge flaps on vane set 6 need to be removed. In the configuration tested in the 1/50th-scale model, two additional flaps were removed in an attempt to ameliorate the effects of the large area change which occurs downstream of the wall. The barrier is located such that if the air-exchange intake door were fully open, 10% of the flow upstream of vane set 6 would pass through the exhaust and the remaining 90% would pass through vane set 6. As the air-exchange door is closed, a decreasing percentage of air flows out the exhaust. Figure 35 is a plot of air-exchange rate as a percentage of test section mass rate of flow versus the position of the intake door as a percentage of the width of the north corridor. On the figure is a family of curves showing the variation of air-exchange performance for several exhaust configurations. The data are taken from full-scale as well as model measurements. It is clear from the figure that the presence of the wall results in only a small reduction in the air-exchange rate compared with the data with the wall removed.

Because of concerns about the ability of the south-end structure to withstand negative-differential wall pressures, a detailed investigation of the pressure distribution in the south end was performed using the 1/50th-scale model. A water manometer was used to make the pressure measurements. The static pressure referenced to atmospheric pressure was measured at three locations on the walls of the model upstream of the acoustic barrier and at four locations downstream of the barrier. Figure 36 shows the locations of the orifices and the results of those measurements. The pressures (reduced to coefficient form and referenced to test-section dynamic pressure) are plotted versus distance along the wind tunnel wall in feet. The uncertainty in the measurements is estimated to be $\pm 0.006 C_{p_{ts}}$ (± 2 lb/ft^2). The southwest corner of the wind tunnel is defined as the origin. The location of the acoustic barrier is shown approximately 18 ft from the origin. The three curves on figure 36 illustrate the distribution of static pressure in this area for 0, 5, and 10% air-exchange rates. Only for the case of 0% air exchange does the pressure coefficient in the south end become negative. The maximum negative pressure based on a test-section dynamic pressure of 262 lb/ft^2 is 8.2 lb/ft^2. Also shown on figure 36 are several data points (solid symbols) from measurements taken with the wall removed and the vane set 6 flaps replaced. Only immediately downstream of the wall is there a significant difference between the wall-in and wall-out data. With the wall installed, the negative pressure in this region is significantly greater. Figure 37 shows the location of the region of reduced

10

static pressure. This occurs only for a 0% air-exchange condition. Figure 38a shows the effect of air-exchange rate on the south-leg wall pressure. The figure is a plot of predicted full-scale pressure differential across the south wall as a function of air-exchange rate. The solid line is based on measurements made with the wall installed. The dashed line represents the current estimate of the south-wall pressure trend without the wall. In both cases, the pressure increases as the intake door is opened. The effect of the wall is most pronounced at the 0% air-exchange condition. At 0% air exchange, the effect of the wall is to decrease the static pressure by approximately 4.5 lb/ft^2 below the level with the wall out. At the maximum air-exchange rate, the wall does not change the differential pressure. Figure 38b is a similar plot for the north-end wall pressure.

Measurements of the static pressure on both sides of the acoustic barrier were made. The pressures were measured at two chordwise locations on the wall; $\frac{x}{c} = 0.24$ and $\frac{x}{c} = 0.61$. The pressures were measured approximately halfway up the wall. Figures 39a and b show the resulting pressure coefficients at these locations for the west and east sides of the acoustic barrier. Figure 40 is a plot of the differential-pressure coefficient versus chordwise location on the wall for three air-exchange conditions. For a test-section dynamic pressure of 262 lb/ft^2, the maximum load on the barrier is expected to be approximately: east to west, 4.6 lb/ft^2 ($\dot{m} = 10\%$) and west to east, 9.8 lb/ft^2 ($\dot{m} = 0\%$).

When the louvers of vane set 7 are closed as in the 40 by 80 mode of operation, small gaps exist along the sides and lower edges of the louvers. These gaps permit a small amount of venting to the atmosphere. This airflow may act to reduce the differential pressure in the south end. The effect of these gaps was simulated in the 1/50th-scale model by opening holes in the south end between vane sets 6 and 8. The scaled area of these openings was representative of the total area of the gaps in the full-scale tunnel. The differences in differential wall pressure with the holes open and then taped shut, though systematic, was within the measurement uncertainty of the water manometer. It was concluded that the vane set 7 gaps would permit only a small reduction in the differential wall pressure in the south end of the wind tunnel.

With the acoustic barrier removed and all of the vane set 6 flaps in place, flow visualization in the 1/50th-scale model revealed a recirculation region immediately downstream from the exhaust opening. This recirculation region was confined to an area adjacent to the south wall. and the width was less than 10% that of the south corridor. When the vane set 6 flaps were removed and the wall was installed, the recirculation region moved away from the south wall toward the centerline of the tunnel. The width of the region increased to approximately 15% of the width of the south corridor. It was believed that the effects of the larger region of recirculation would persist into the test section and adversely affect the flow quality there. Subsequent model tests reduced this concern.

Figure 41a presents a comparison of the lateral distribution of dynamic pressure in the test section at 0% air exchange for the wall-in and wall-out configurations. The west

11

or courtyard side of the test section is shown on the right of the figure and the east side is shown on the left. The rectangle in the figure indicates the design goal for test section flow uniformity in the horizontal direction ($\pm 0.5\%$ of the average dynamic pressure over 75% of the test section). For this air-exchange condition, the presence of the acoustic barrier does not adversely affect the dynamic pressure distribution. Figure 41b presents a similar comparison for a 5% air-exchange condition. In this case, the dynamic-pressure distribution with the wall installed is within specification over approximately the middle 30% of the test section. Approximately 50% of the test section is within specification for the case with the wall removed. Figure 41c shows a comparison of the dynamic pressure distributions for the 10% air exchange condition. The curve for the wall-in case is within specification over nearly the entire width of the test section. The distribution for the wall-out case is within specification over the western 80% of the test section. With the exception of the wall-in, 5% air-exchange case, the lateral distribution of dynamic pressure in the test section is well within specification.

Figure 42 presents a comparison of the distributions of lateral turbulence intensity in the test section of the 1/50th-scale model for the wall-in and wall-out configurations. A third curve on the figure shows the turbulence intensity distribution with the wall in and the flaps on the two vanes immediately to the east of the wall reinstalled. In all cases, the air-exchange rate was set at 10% . A single hot wire, oriented vertically, was traversed across the test section to make these measurements. Because of the orientation of the wire, the actual turbulence measured was the resultant intensity in the horizontal plane, $\sqrt{(\bar{u'})^2 + (\bar{v'})^2}$. The design goal for the resultant turbulence intensity in the horizontal plane is 0.63% over 75% of the width of the test section. This level is shown on the figure. The wall-in, no-flap configuration satisfies the flow-quality specification. Adding the flaps to the vanes adjacent to the wall results in a pronounced east-to-west gradient of turbulence intensity. Removing the wall results in a small portion of the east side turbulence distribution exceeding the flow quality specification. No measurements were made of the turbulence intensity distributions for the 0 and 5% air exchange conditions.

CONCLUSION

A 1/50th-scale model of the 40- by 80-Foot Wind Tunnel located at NASA Ames Research Center was tested in a configuration which simulated the 1986 operational configuration of the full-scale facility. Of particular interest in these tests were the debris screen and supporting superstructure which will be installed on the air-exchange intake and exhaust openings of the full-scale wind tunnel and the acoustic barrier located next to the exhaust openings near vane sets 6 and 7. The changes in the characteristics of these

openings reduced the air-exchange rate only slightly. The static pressure balance in the wind tunnel circuit was also only changed slightly.

Total-pressure contours in the flow field were generated from rake surveys made at various locations around the circuit. The surveys documented the existence of a large wake generated by the primary-diffuser ceiling-support struts. The surveys also documented the flow field downstream of the air-exchange intake door and in the south end of the wind tunnel as the air-exchange rate was varied.

The 1/50th-scale model was also used to investigate the aerodynamic effects of the installation of the acoustic barrier in the southwest corner of the wind tunnel. The primary effect of the acoustic barrier is to decrease the static pressure in the wind tunnel at the zero air exchange condition. A secondary effect of the barrier is to locally decrease the static pressure downstream of vane set 6 near the southwest corner of the circuit. The air-exchange rate and test section flow quality were essentially unchanged because of the installation of the acoustic barrier.

REFERENCES

1. Schmidt, Gene I.; Rossow, Vernon J.; Van Aken, Johannes; and Parrish, Cynthia L.: One-Fiftieth-Scale Model Studies of 40- by 80-Foot and 80- by 120-Foot Wind Tunnel Complex at NASA Ames Research Center. NASA TM 89405, 1987.

2. Rossow, V. J.; Schmidt, G. I.; Meyn, L. A.; Ortner, K. A.; and Holmes, R., E.: Aerodynamic Characteristics of an Air-Exchange System for the 40- by 80-Foot Wind Tunnel at Ames Research Center. NASA TM 88192, 1986.

3. Corsiglia, V. R.; Olson, L. E.; and Falarski, M. D.: Aerodynamic Characteristics of the 40- by 80-/80- by 120-Foot Wind Tunnel at NASA Ames Research Center. NASA TM 85946, 1984.
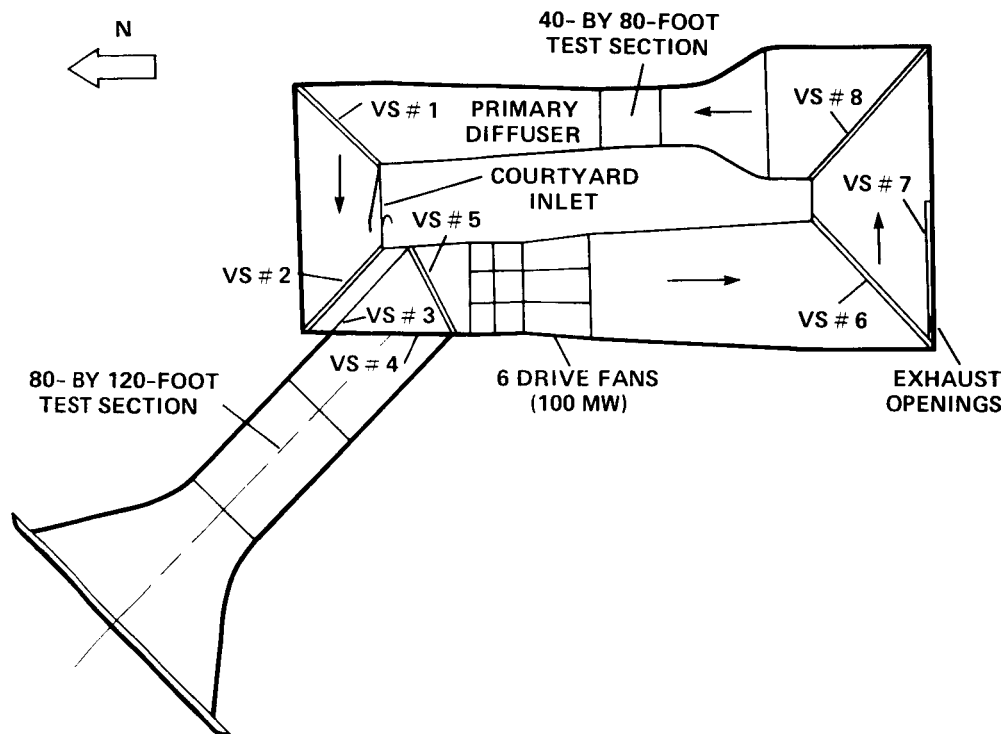
Figure 1.- Plan view of the NFAC at NASA Ames Research Center which illustrates the 40- by 80-ft and 80- by 120-ft wind tunnel circuits.
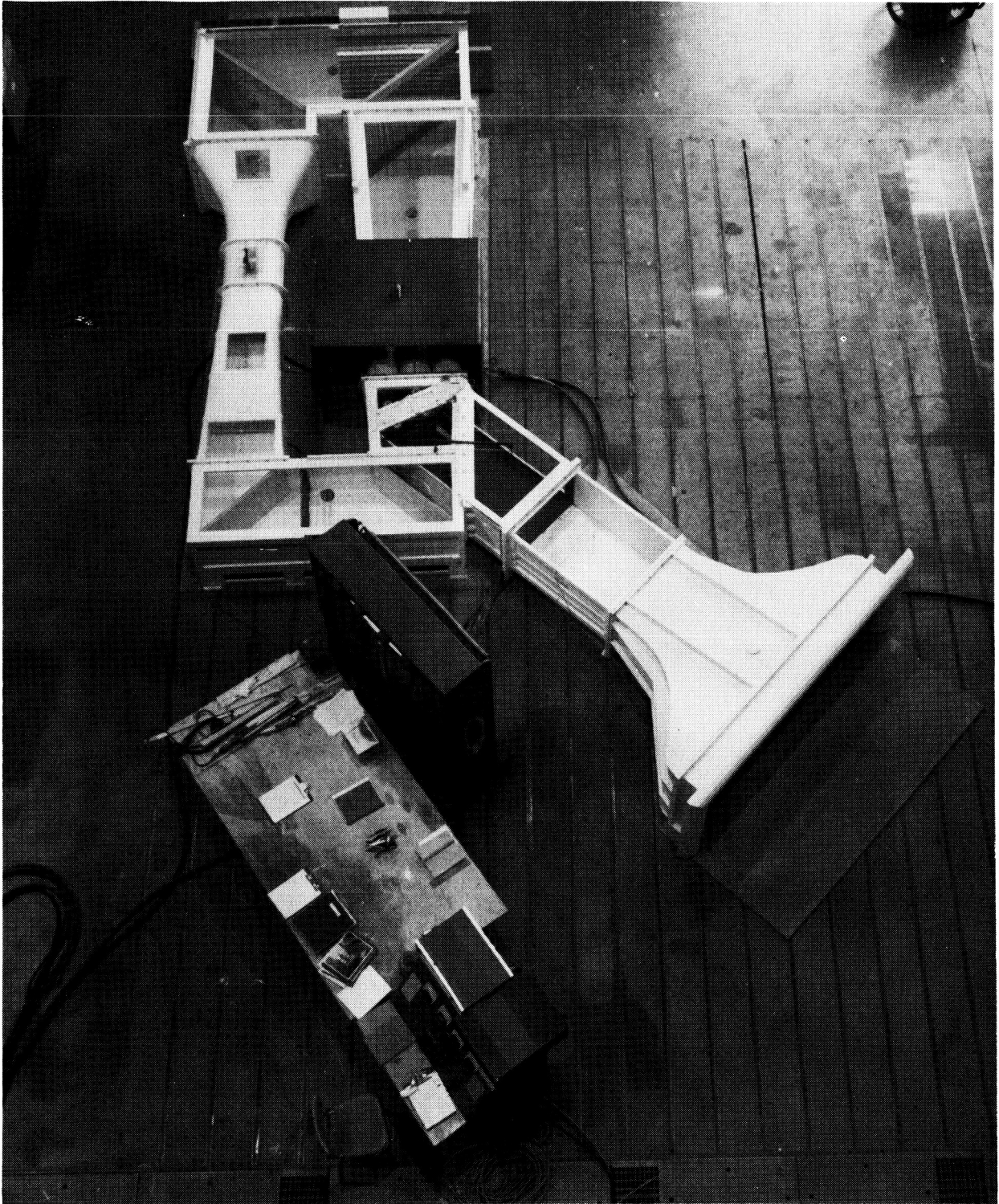
Figure 2.- One-fiftieth-scale 40- by 80- by 120-ft wind tunnel model.
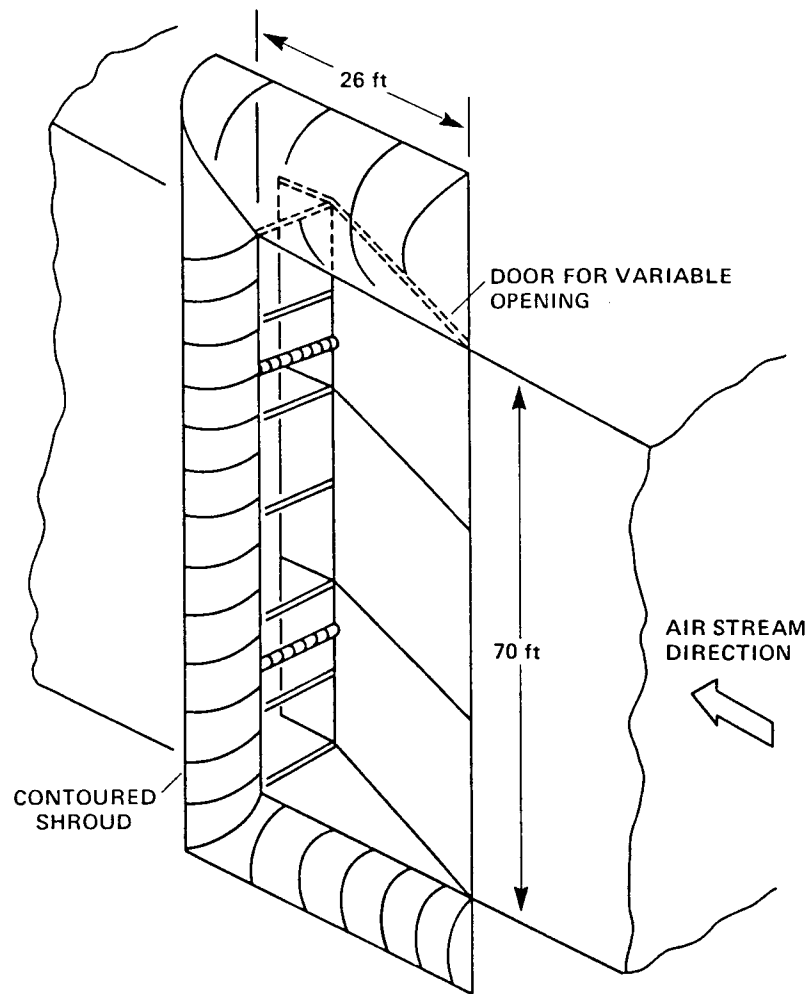
Figure 3.- Air-exchange inlet of 40 by 80.
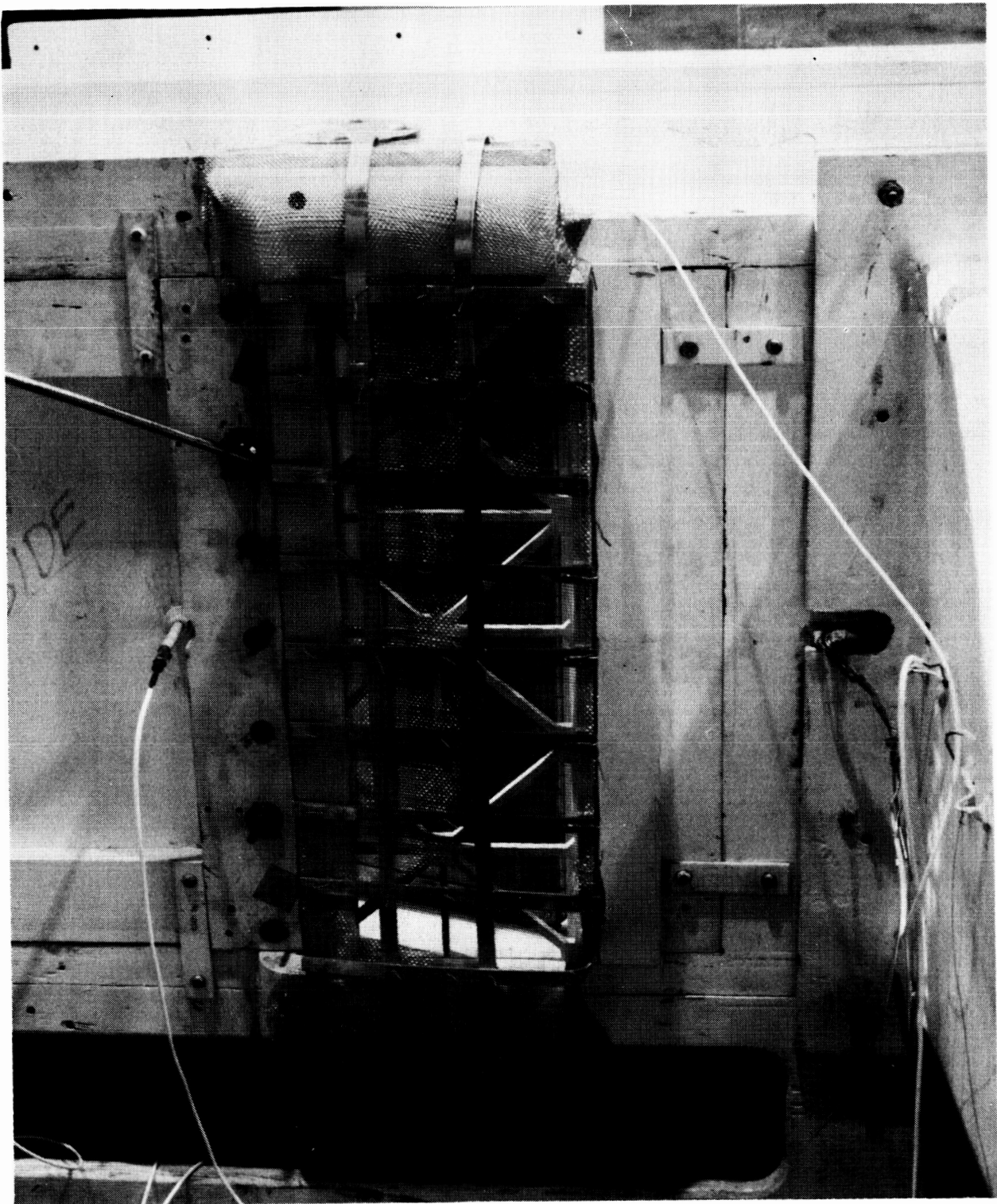
Figure 4.- External view of air-exchange inlet of 1/50th-scale model of 40 by 80.
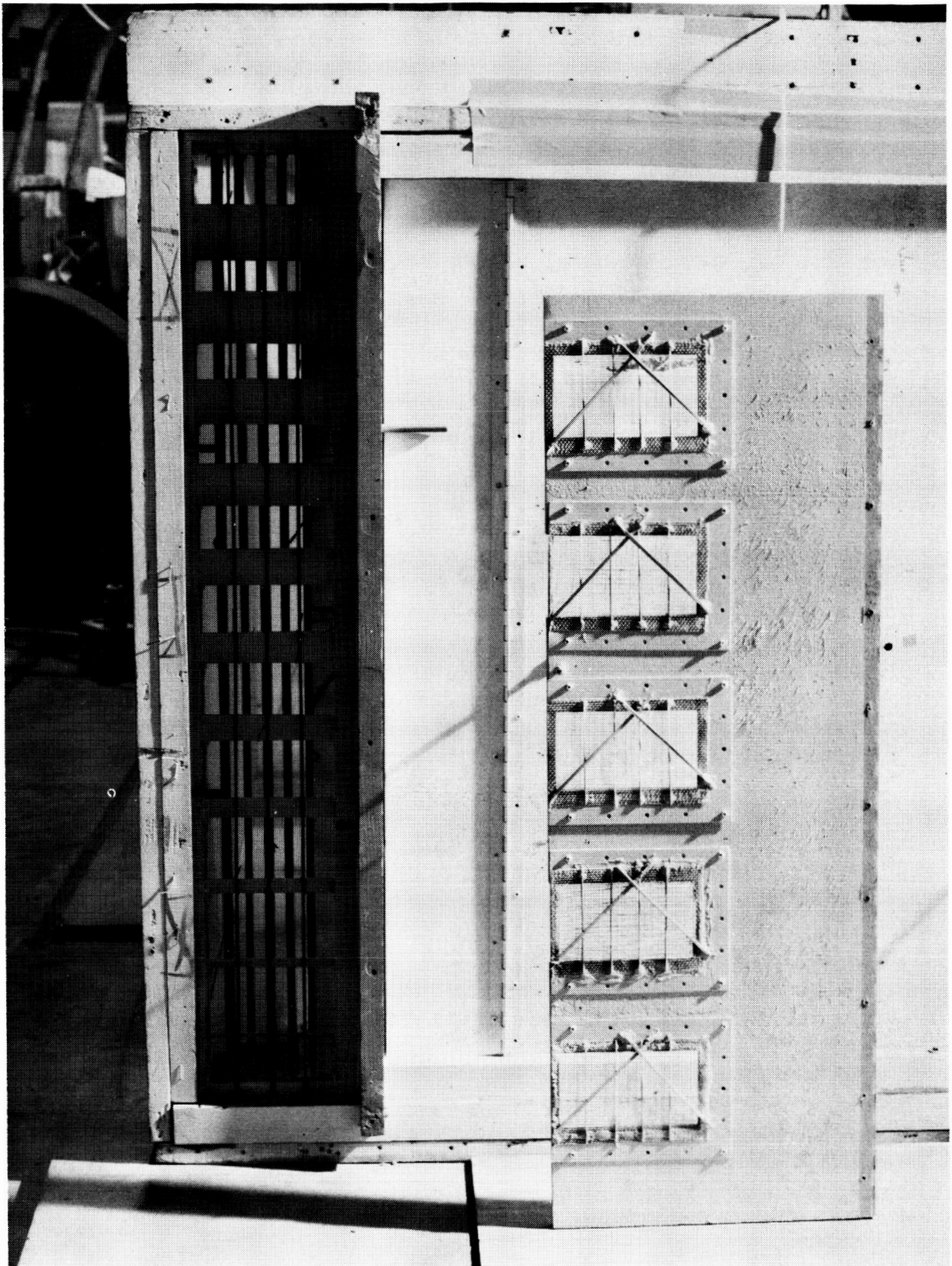
Figure 5.- External view of air-exchange exhaust of 1/50th-scale model of the 40 by 80 showing 5-door and fully open west column.

A'

**DIRECTION OF
INDUCED FLOW**

D

₵ | 1/2D | D

CROSS-SECTION OF PRIMARY DIFFUSER

α
$\alpha = 15°$
$\pm 1°$

A' ————————————————————————— **A'**

① ② ③ ④ ⑤ ⑥ ⑦ ⑧

CIRCUMFERENTIAL LAYOUT

FLOW DIRECTION

**TEST
SECTION** ←→ **PRIMARY DIFFUSER**

RAMP

**ACOUSTIC
LINER**

**VORTEX
GENERATOR**

—— 12' ± 2' ——

STREAMWISE LOCATION OF VORTEX GENERATORS
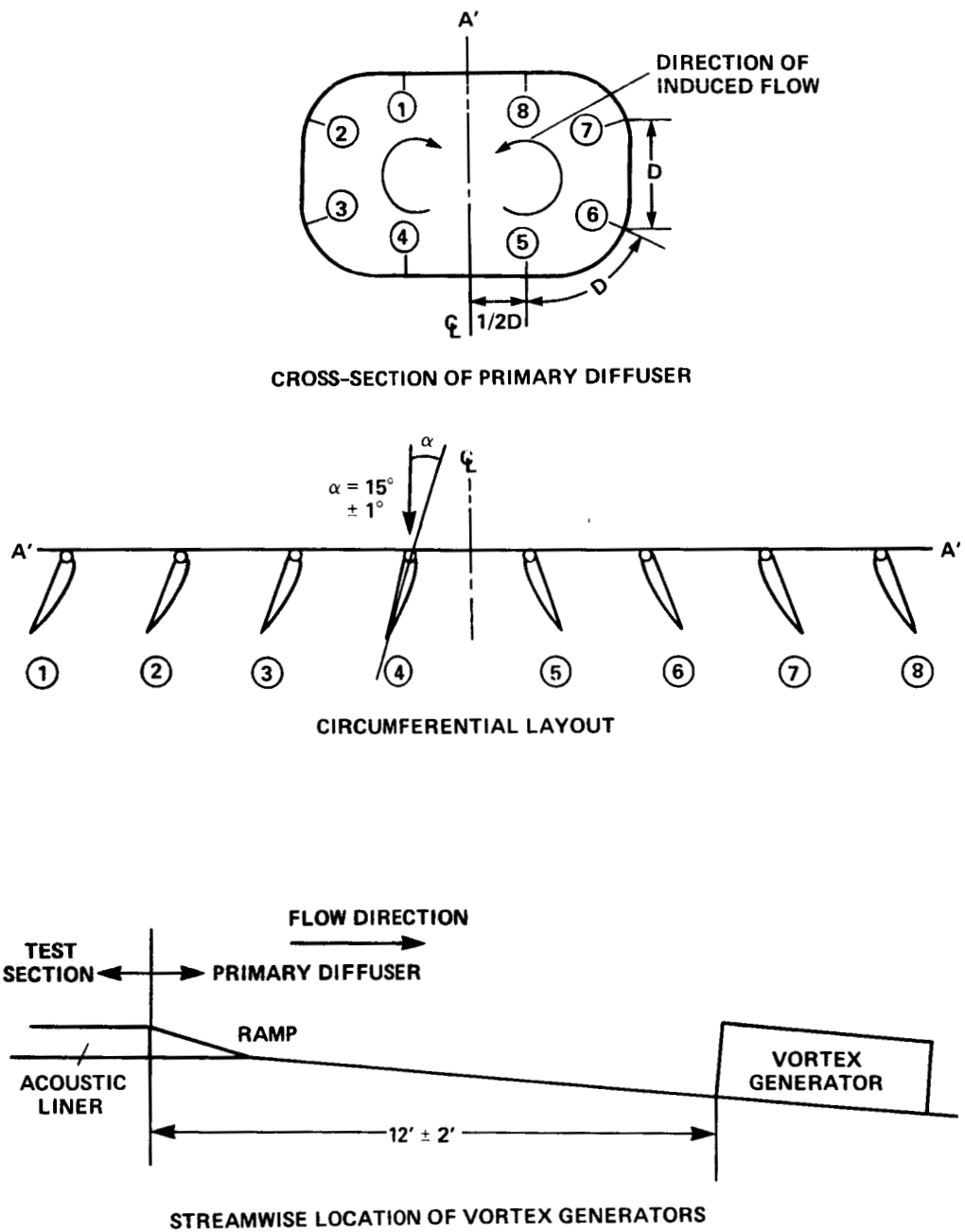
Figure 6.- Location of vortex generators in the 40 by 80 primary diffuser.

19
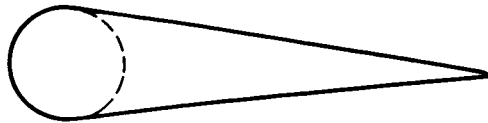
a) FAIRED CYLINDER CONTOUR
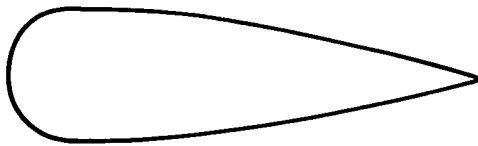
b) FULL-SCALE STRUT CONTOUR

Figure 7.- Airfoil contours of the primary-diffuser ceiling support struts used in the 1/50th-scale model of the 40 by 80. (a) Faired cylinder contour. (b) Full-scale strut contour.

P_S, UPSTREAM STATIC RING

P_S, DOWNSTREAM STATIC PRESSURE

TEST SECTION

AIR FLOW

CONTRACTION TO TEST SECTION

BEGINNING OF CONTRACTION
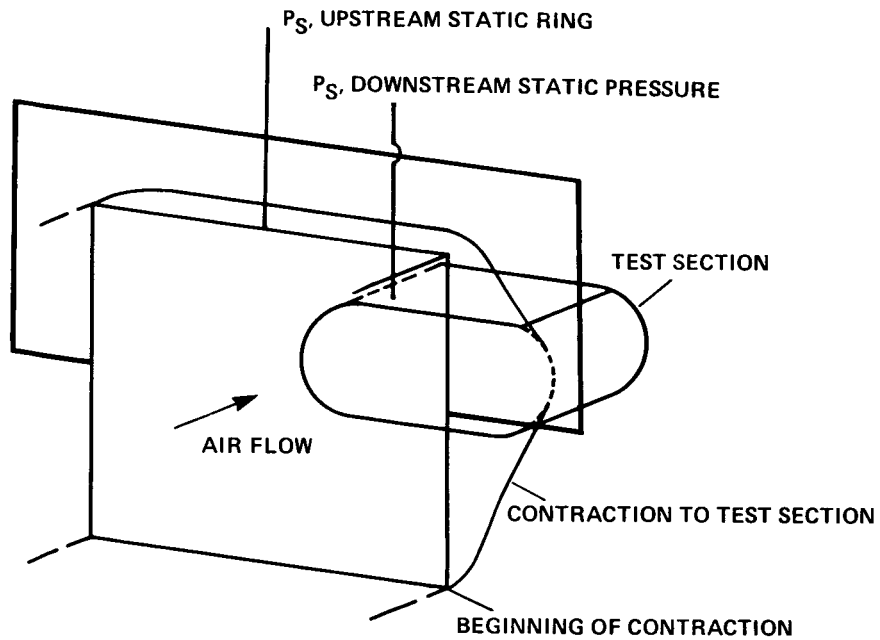
Figure 8.- Connection of upstream and downstream static rings on the contraction of the 1/50th-scale model of the 40 by 80.
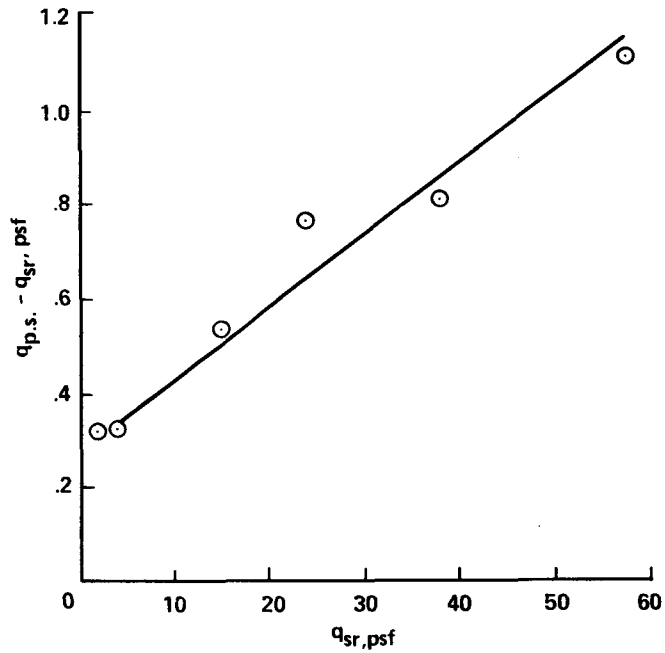
Figure 9.- Difference in dynamic pressure between that measured with the test-section pitot-static probe and the static rings versus test-section dynamic pressure (10% air exchange).
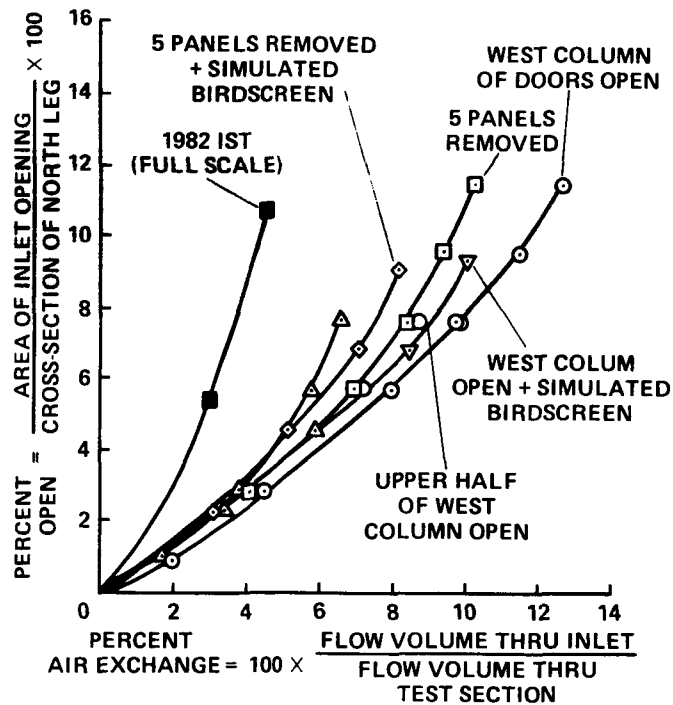
Figure 10.- Opening of courtyard inlet required to obtain a given air-exchange rate for several exhaust configurations (open symbols denote 1/50th-scale data).
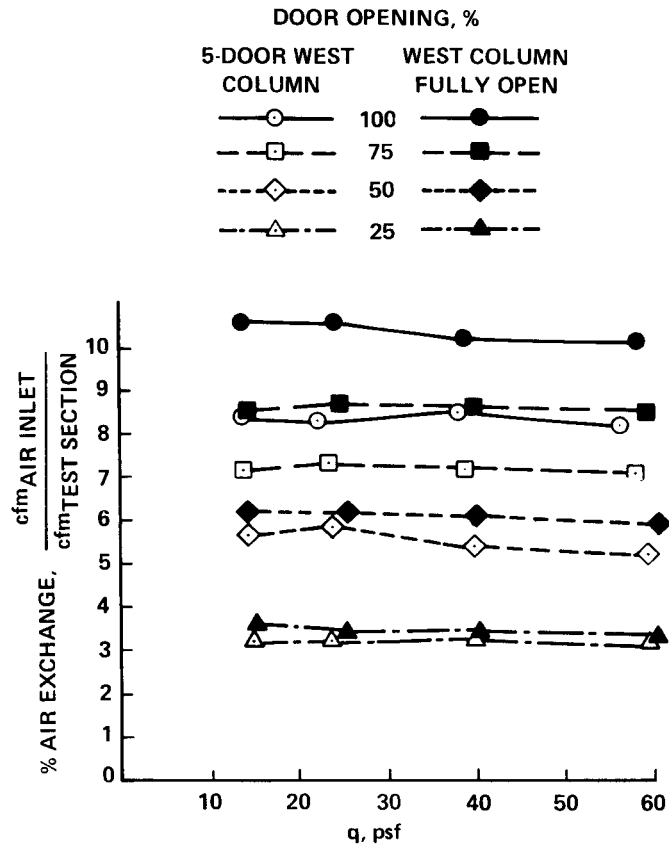
Figure 11.- Test-section dynamic-pressure percentage of air exchange α vs q for four inlet door positions.

○ INDICATES LOCATIONS OF STATIC PRESSURE MEASUREMENT
◎ INDICATES LOCATIONS AT WHICH PRESSURES WERE MEASURED ON BOTH THE CEILING AND THE FLOOR
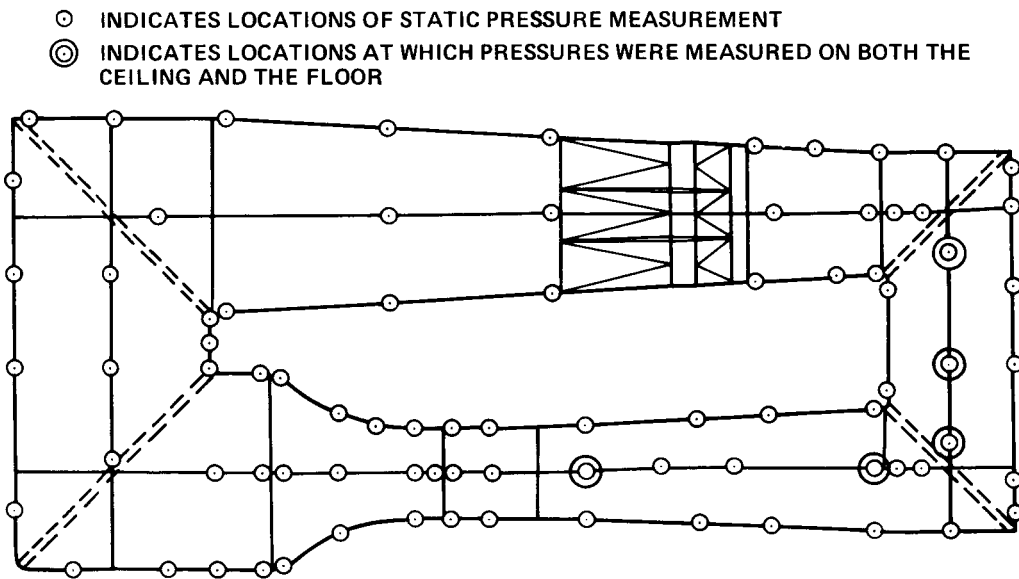
Figure 12.- Locations of static pressure measurements on the 1/50th-scale 40 by 80.

22
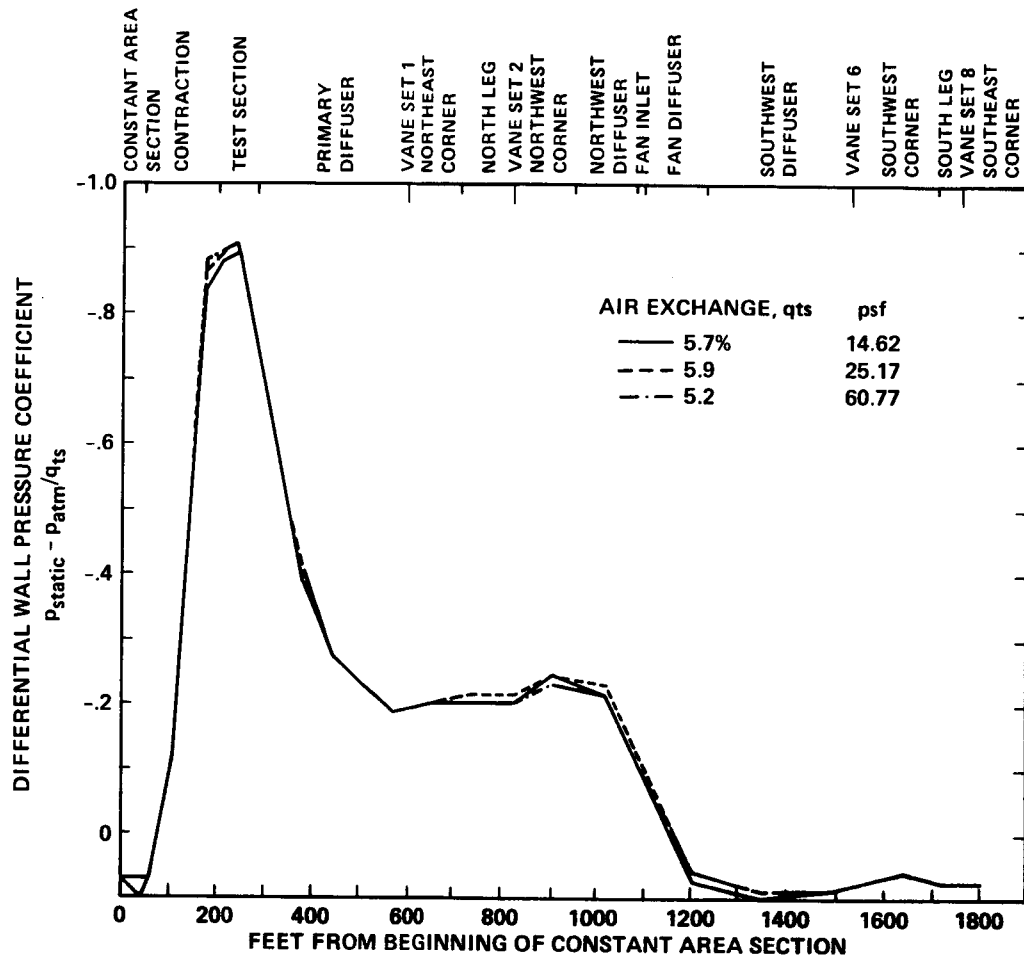
Figure 13.- Differential wall-pressure coefficient variation versus distance around circuit, five-door west column, 6% air exchange.
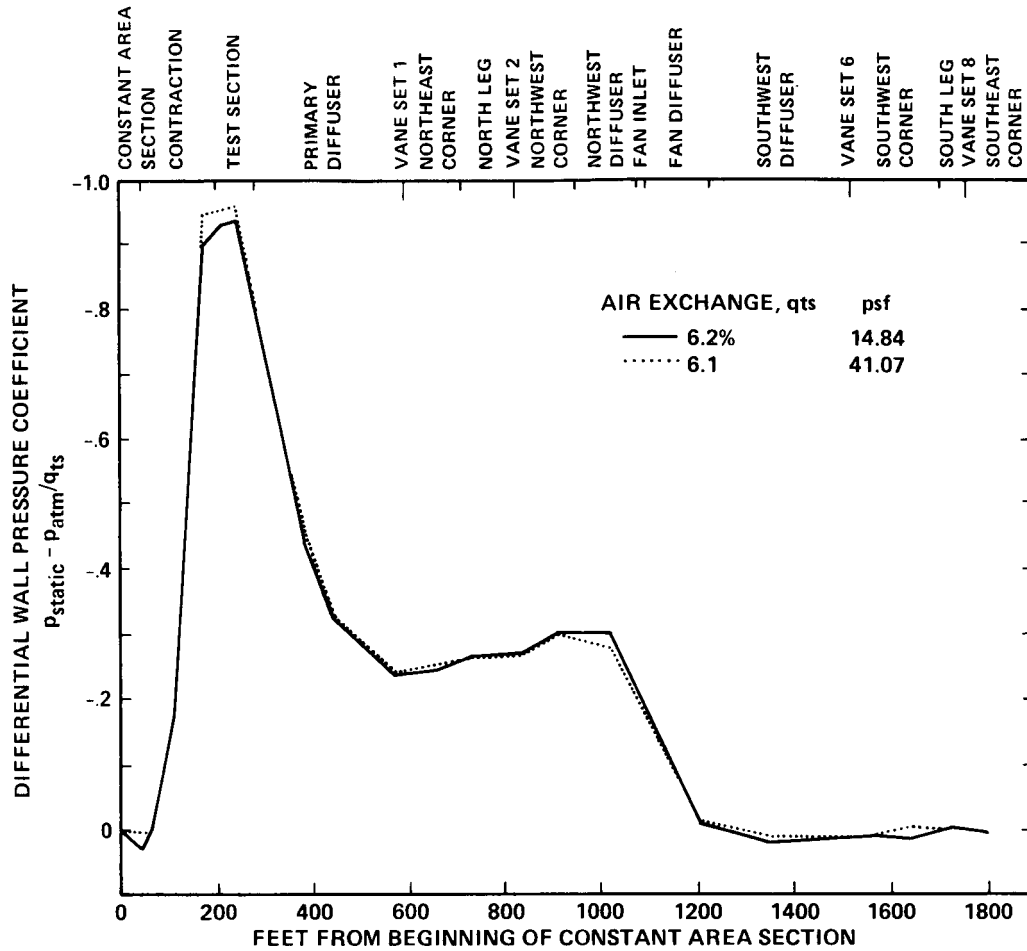
Figure 14.- Differential wall-pressure coefficient variation versus distance around circuit, open west column, 6% air exchange.
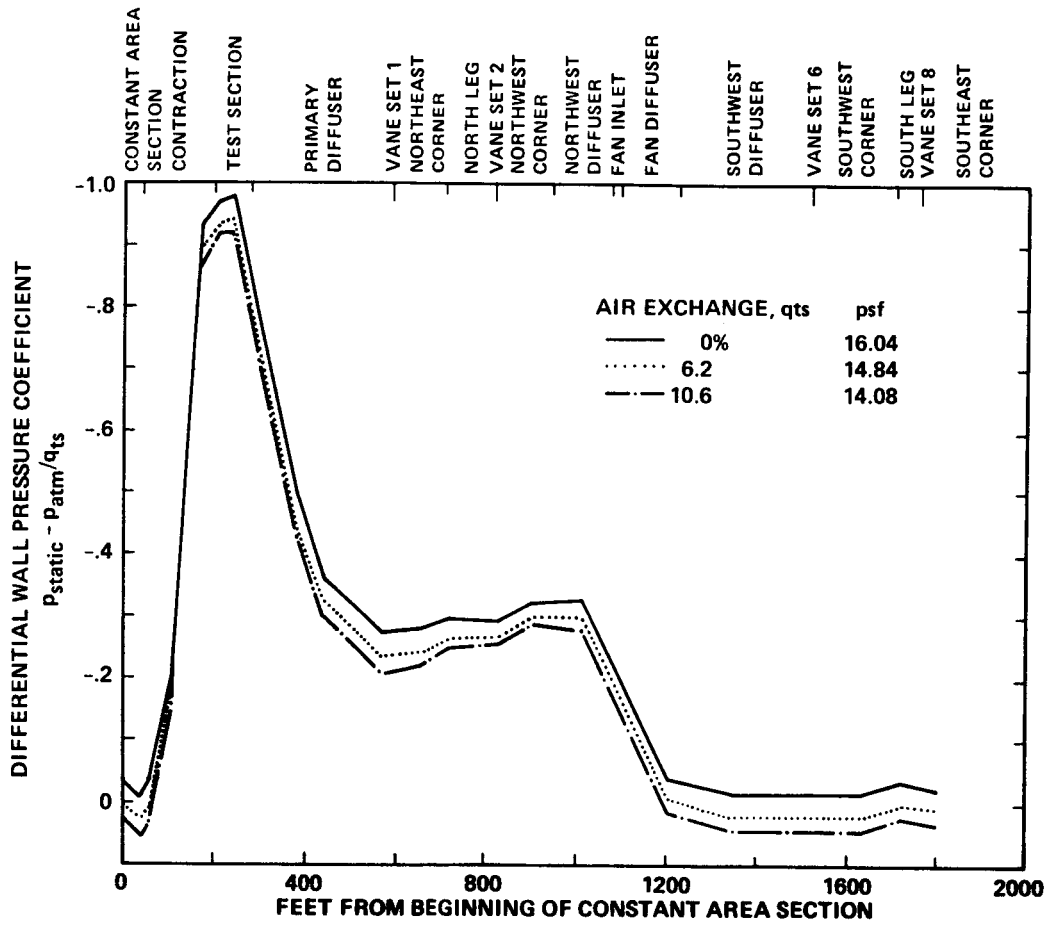
Figure 15.- Differential wall-pressure coefficient variation versus distance around circuit, open west column.
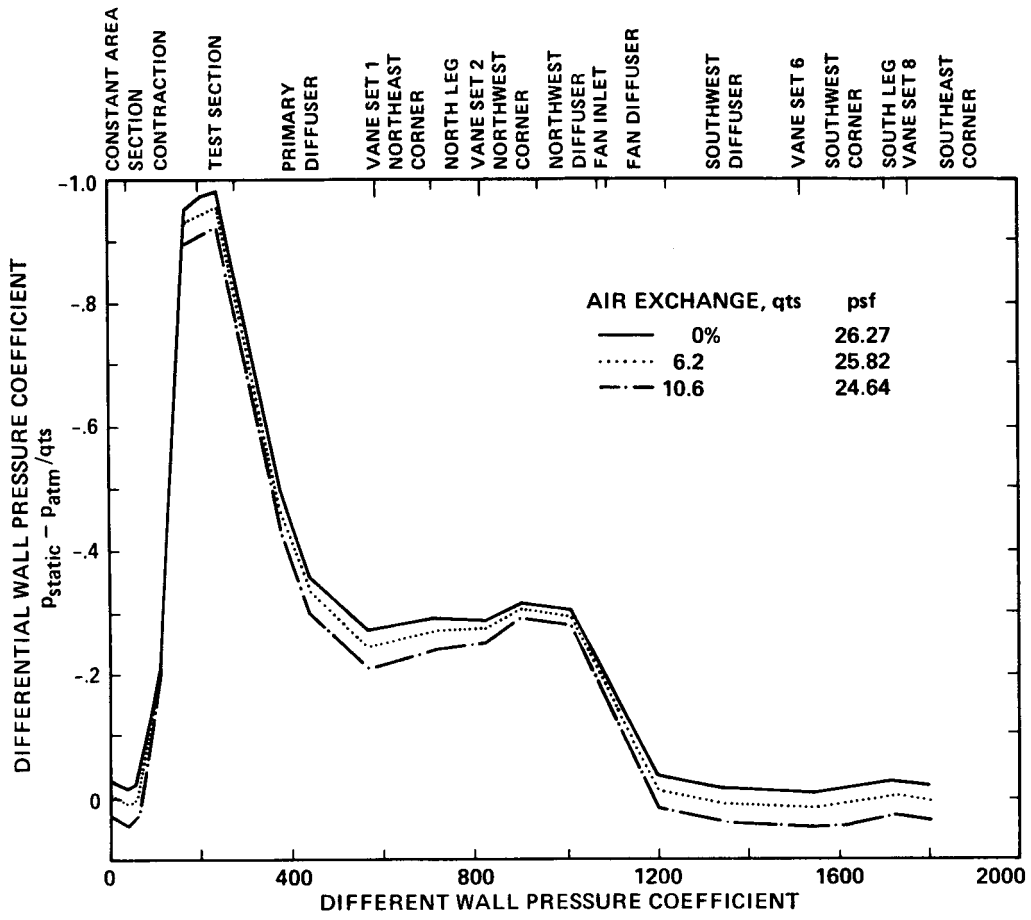
Figure 16.- Differential wall-pressure coefficient variation versus distance around circuit, open west column.
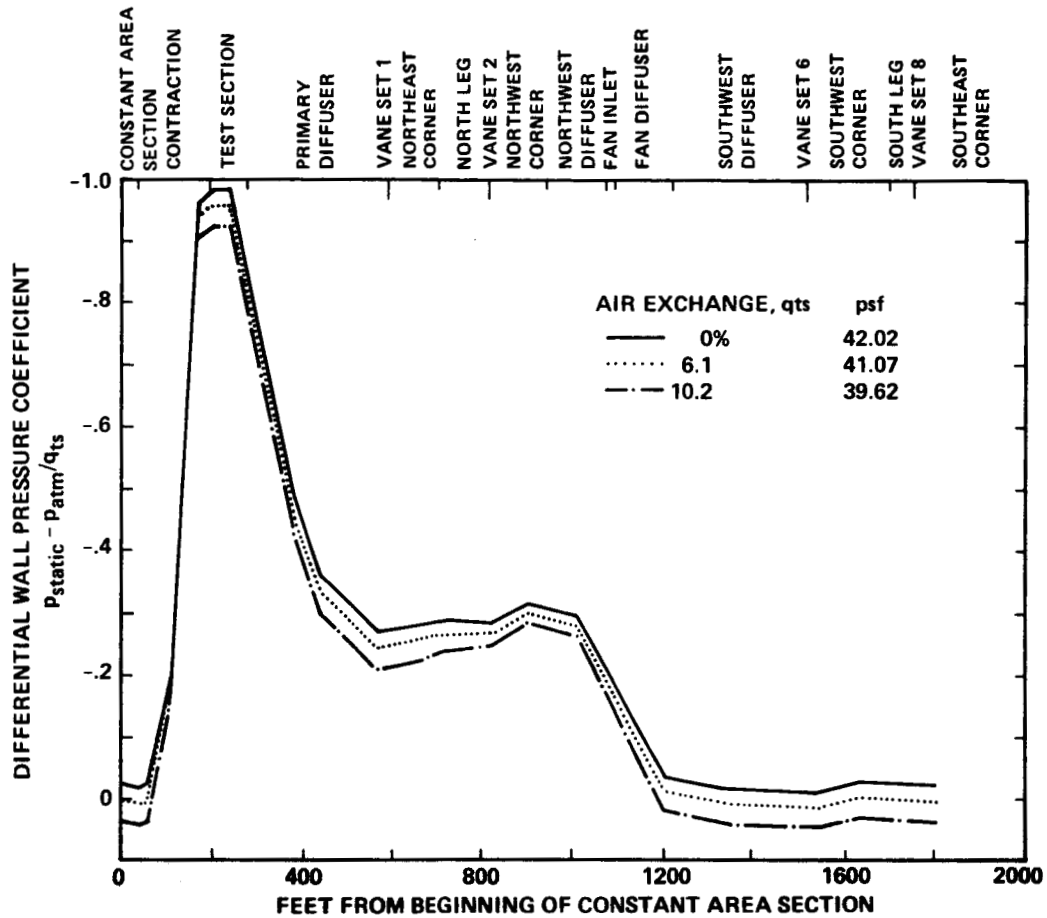
Figure 17.- Differential wall-pressure coefficient variation versus distance around circuit, open west column.

27
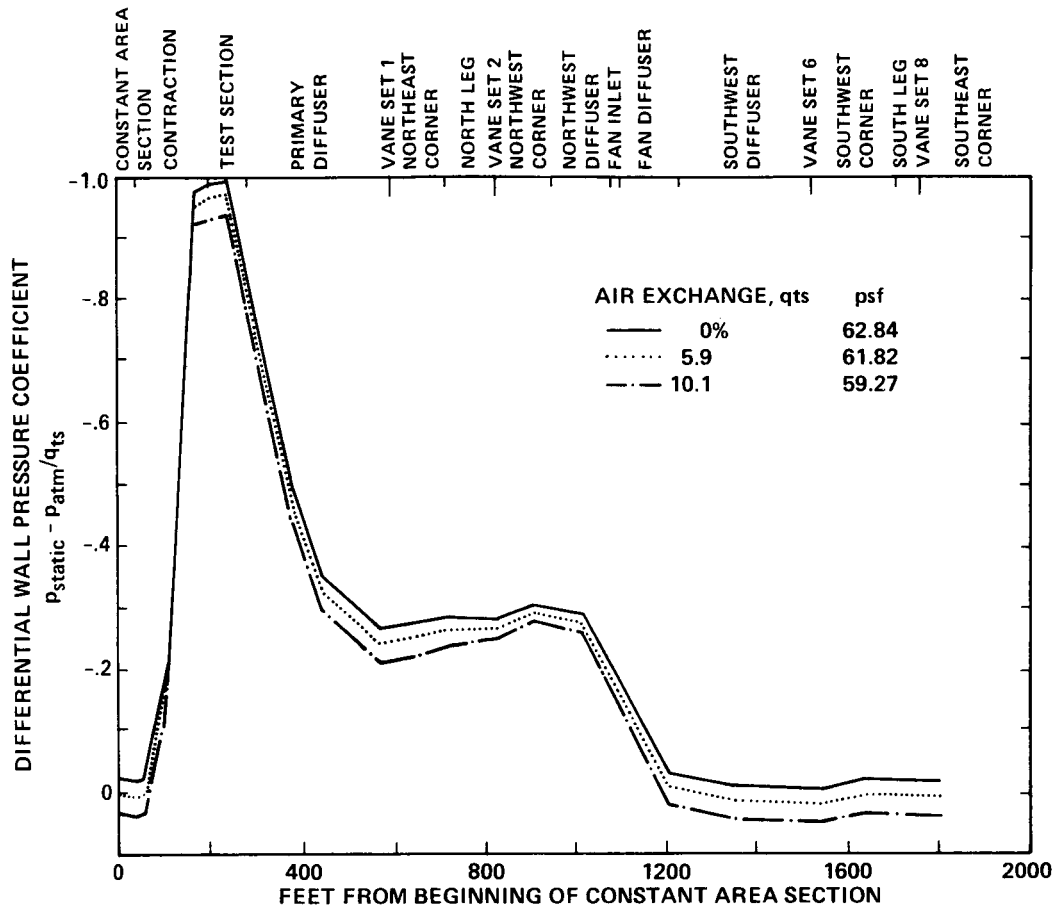
Figure 18.- Differential wall-pressure coefficient variation versus distance around circuit, open west column.
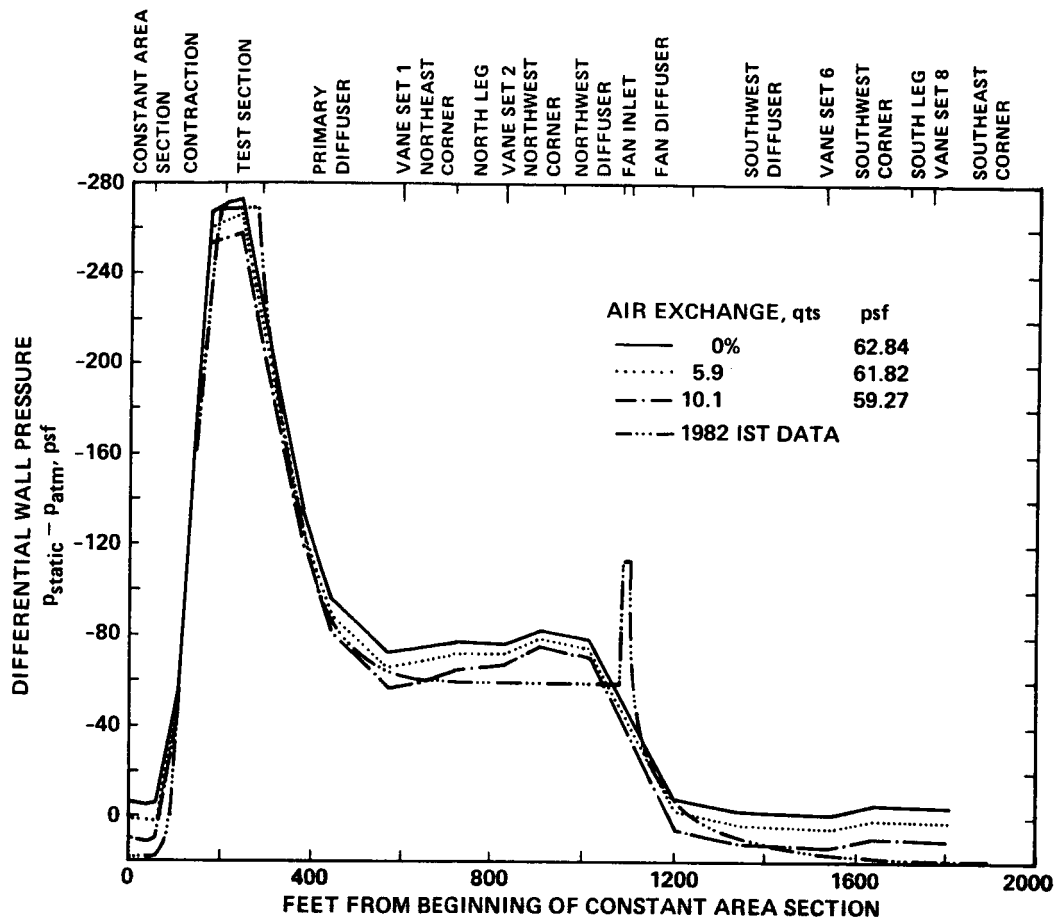
Figure 19.- Predicted full-scale circuit pressures versus distance around circuit, open west column.
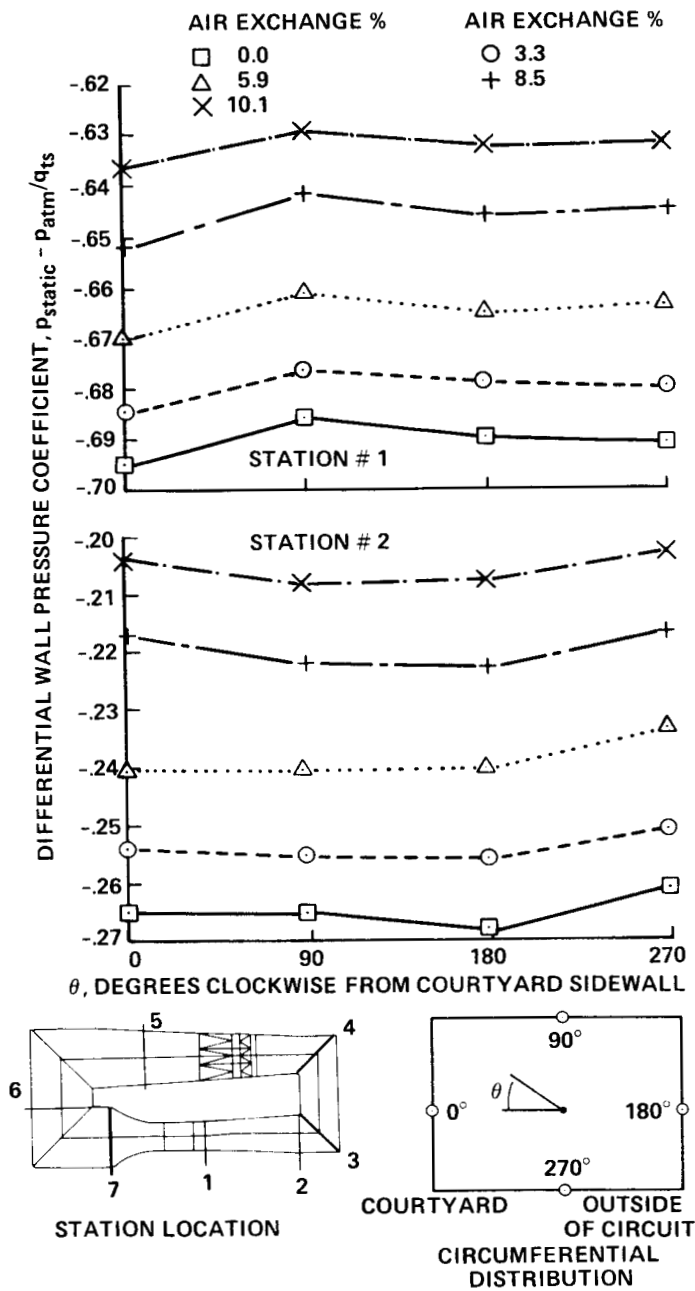
Figure 20.- Cross-sectional wall pressure variation. (a) Station 1. (b) Station 2.
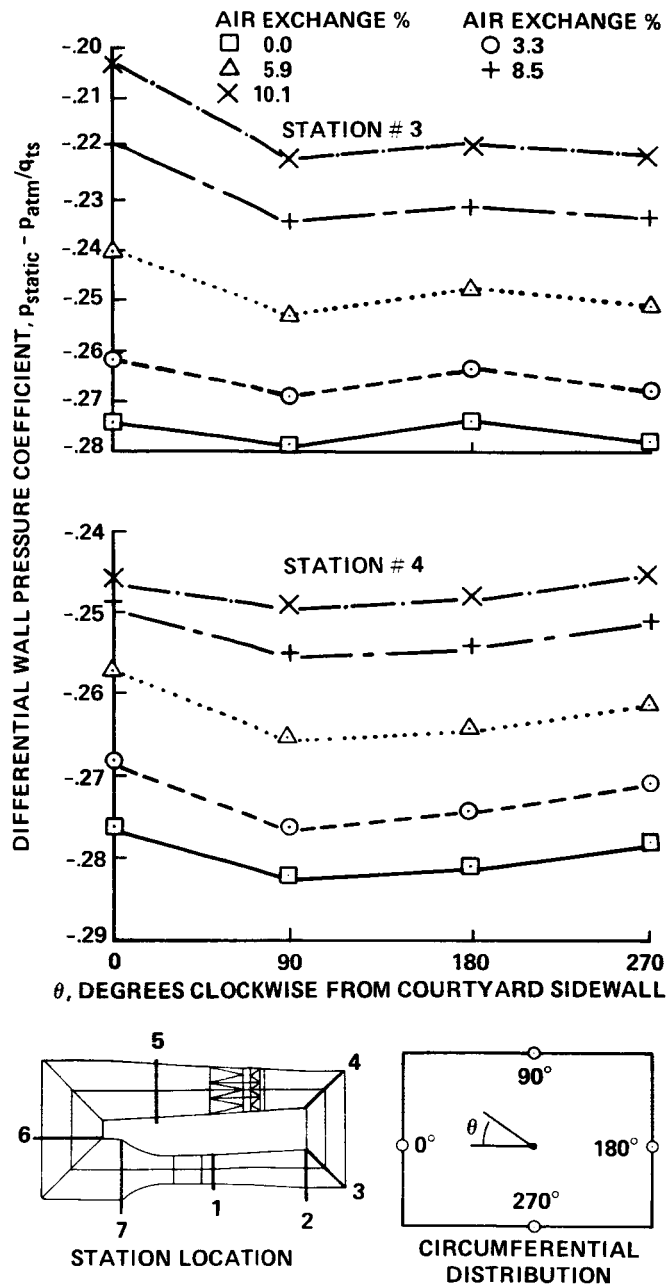
Figure 21.- Cross-sectional wall pressure variation. (a) Station 3. (b) Station 4.
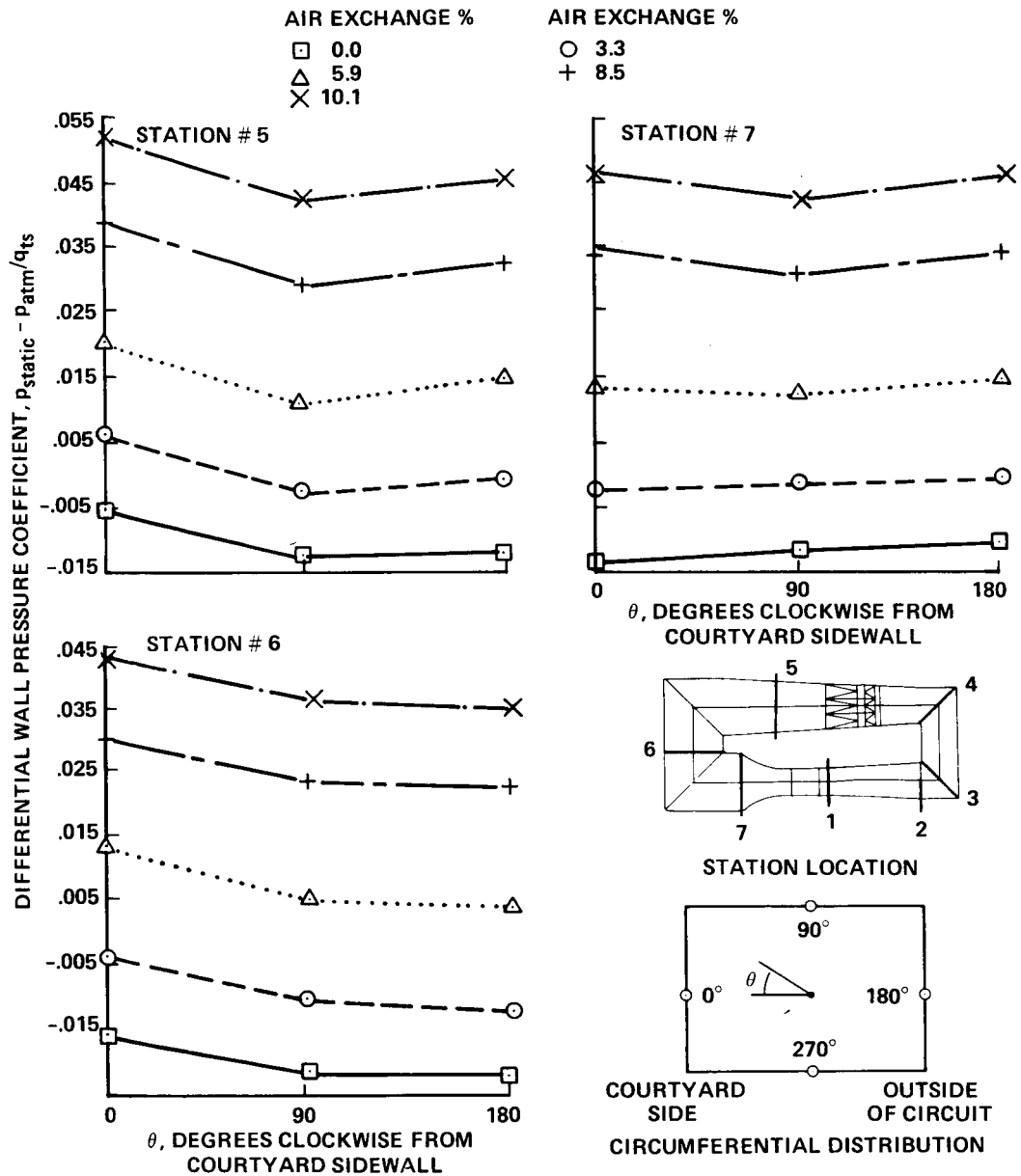
Figure 22.- Cross-sectional wall pressure variation. (a) Station 5. (b) Station 6. (c) Station 7.

32
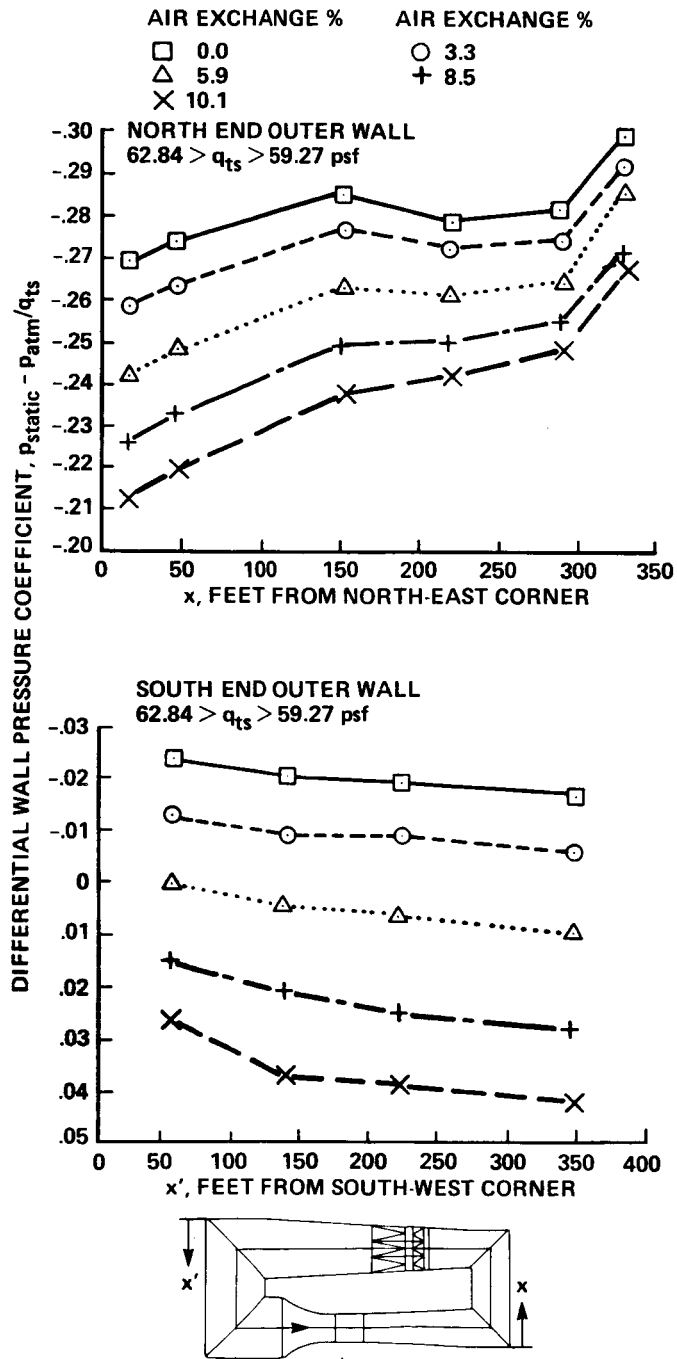
Figure 23.- Wall pressure variation along the north and south outer walls of the 1/50th-scale model of the 40 by 80. (a) North end outer wall, 62.84 ¿ q_{ts} ¿ 59.27 psi. (b) South end outer wall, 62.84 ¿ q_{ts} ¿ 5.27 psi.
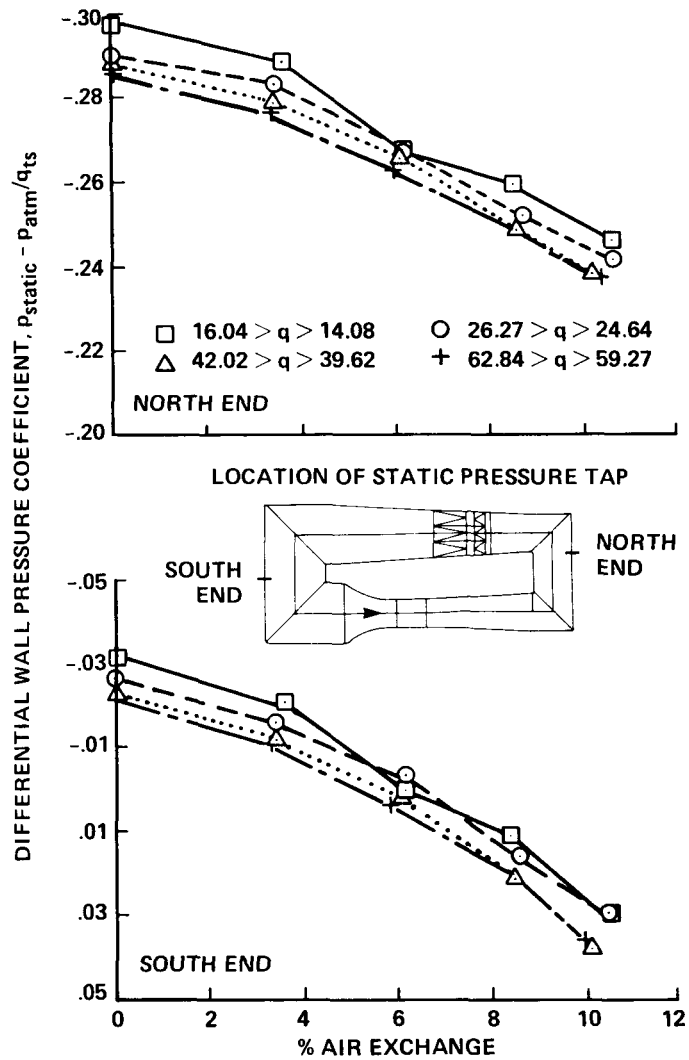
Figure 24.- Change in the north and south end pressures with the air-exchange rate of the 1/50th-scale model of the 40 by 80. (a) North end. (b) South end.

34
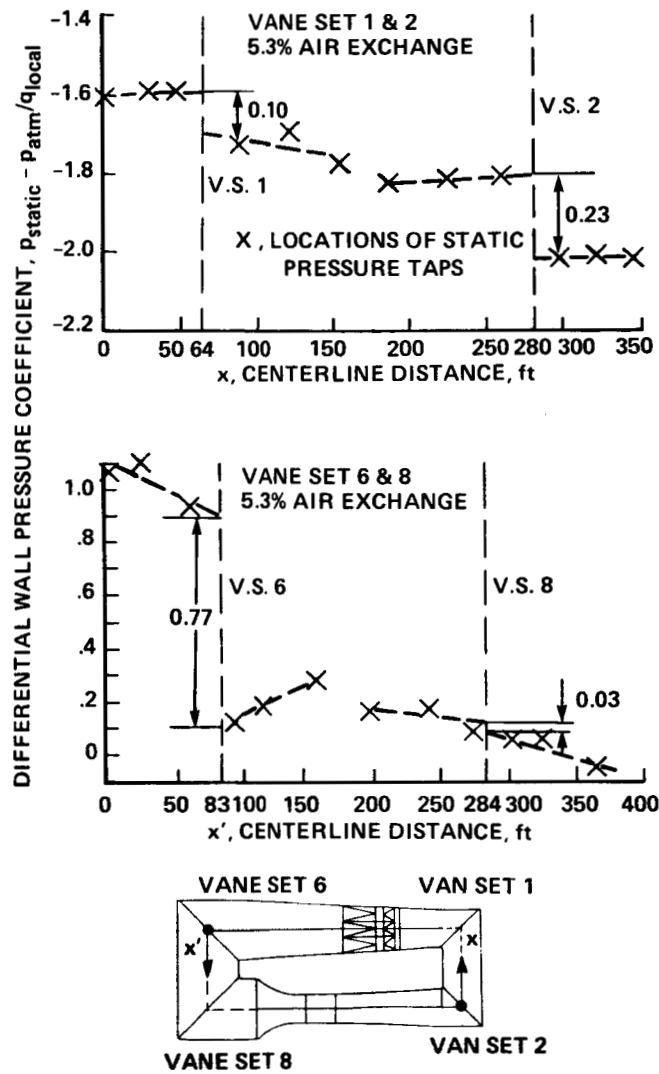
Figure 25.- Graphical estimation of the total pressure loss coefficients of the flow turning vanes of the 1/50th-scale model of the 40 by 80. (a) Vane sets 1 and 2, 5.3% air change. b) Vane sets 6 and 8, 5.3% air exchange.

35

AIR EXCHANGE, % q_{ts}

—————— 0.0   26.27

— — — — 6.2   25.82

- - - - - - - 10.6   24.64

OPEN WEST COLUMN — LOOKING UPSTREAM

EAST SIDEWALL   COURTYARD SIDEWALL

AIR EXCHANGE, % q_{ts}

$\times$ 0.0   62.84

— — —   5.9   59.27

- - - - -   10.1

LOCATION OF CROSS-STREAM SURVEY
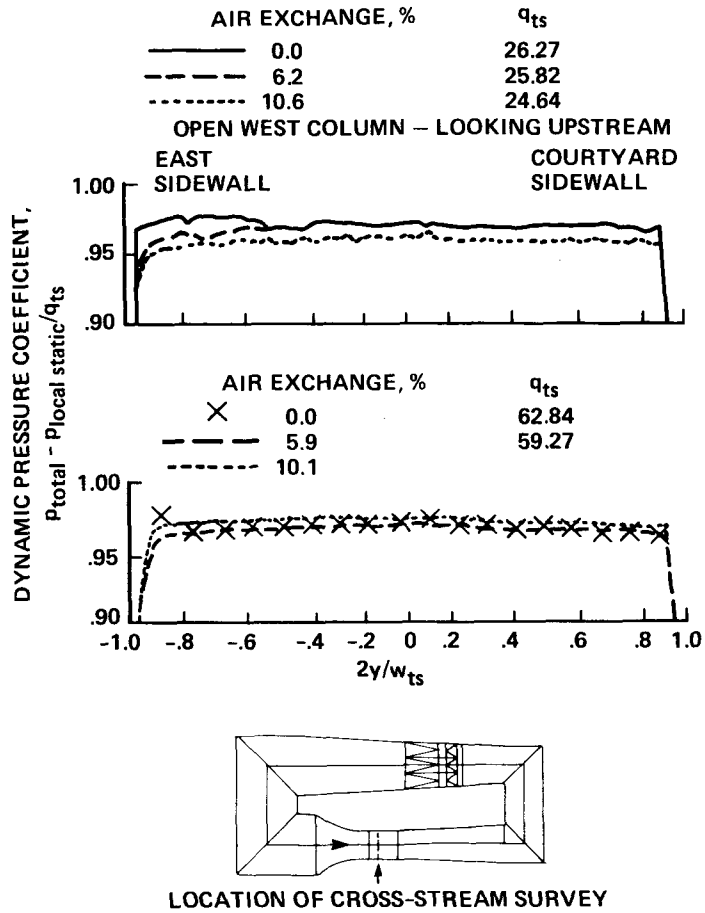
Figure 26.- Distribution of the dynamic pressure coefficient across the test section of the 1/50th-scale model of the 40 by 80. (a) Open west column, looking upstream. (b) Open west column, looking upstream.
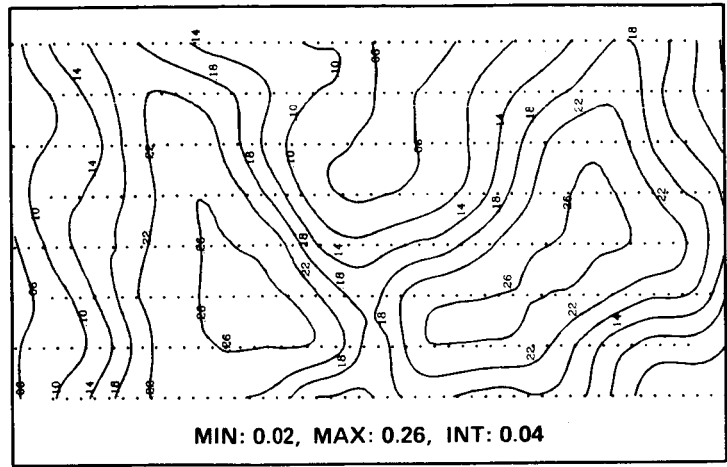
36

MIN: 0.02, MAX: 0.26, INT: 0.04

LOOKING UPSTREAM   **5.9% AIR EXCHANGE**

MIN: 0.02, MAX: 0.26, INT: 0.04
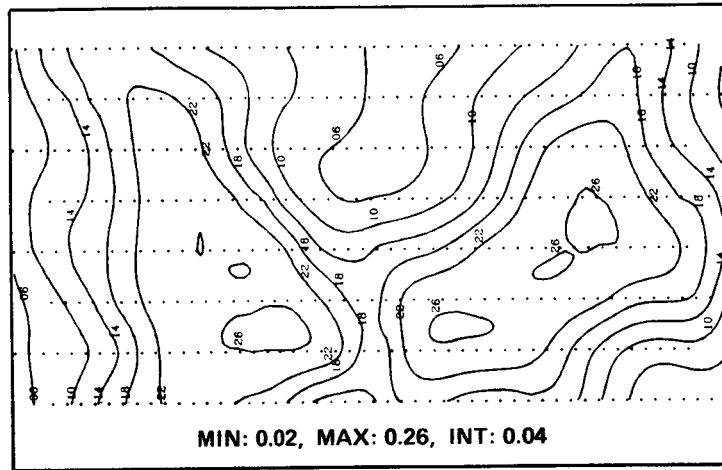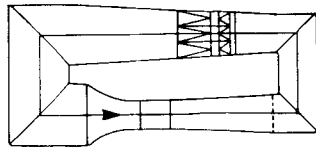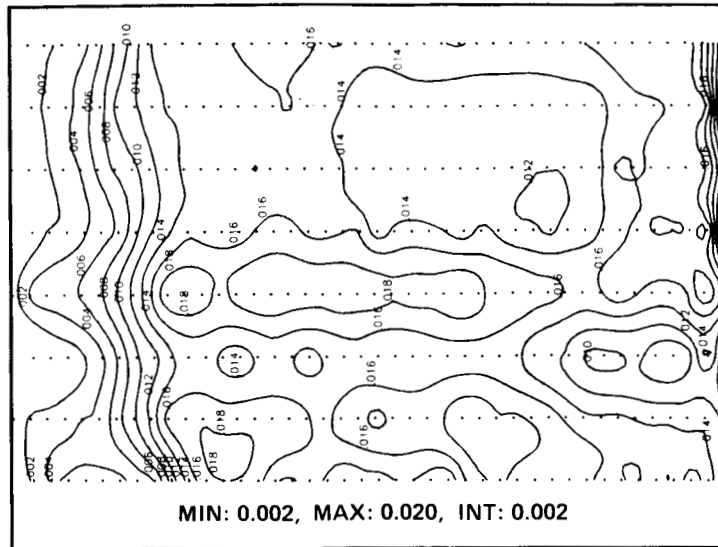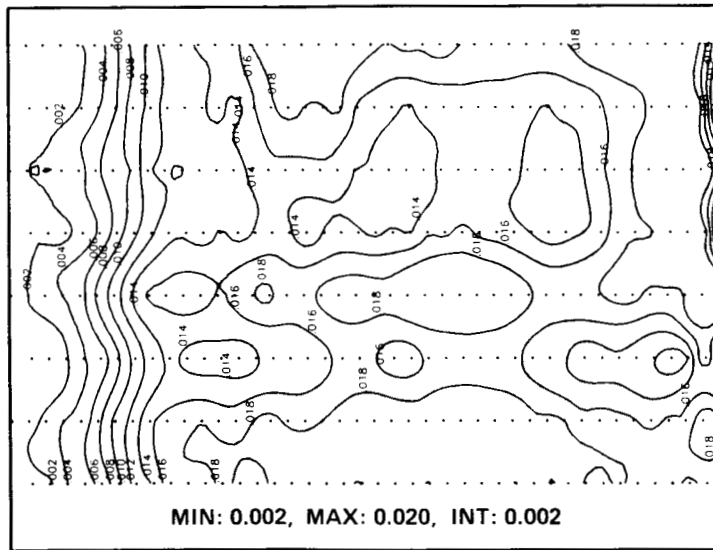
10.1% AIR EXCHANGE

LOCATION OF CROSS-STREAM SURVEYS

Figure 27.- Contours of the dynamic pressure coefficient at the downstream end of the primary diffuser of the 1/50th-scale model of the 40 by 80. (a) 5.9% air exchangge. (b) 10.1% air exchange.
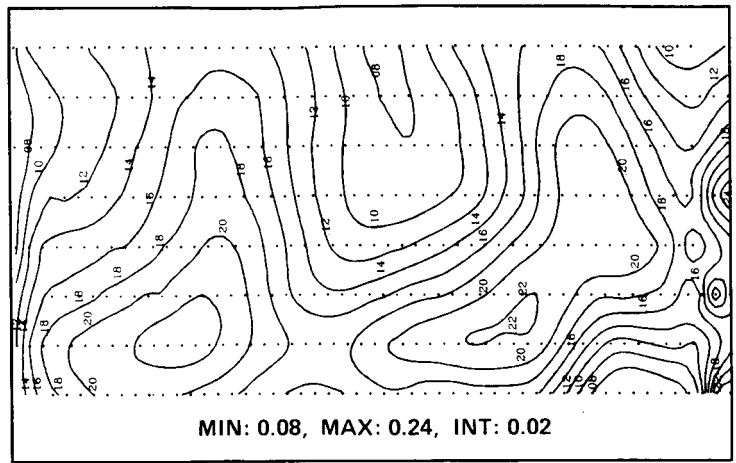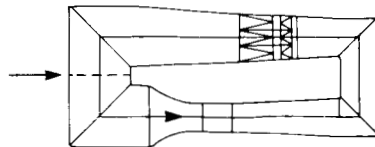
MIN: 0.08, MAX: 0.24, INT: 0.02
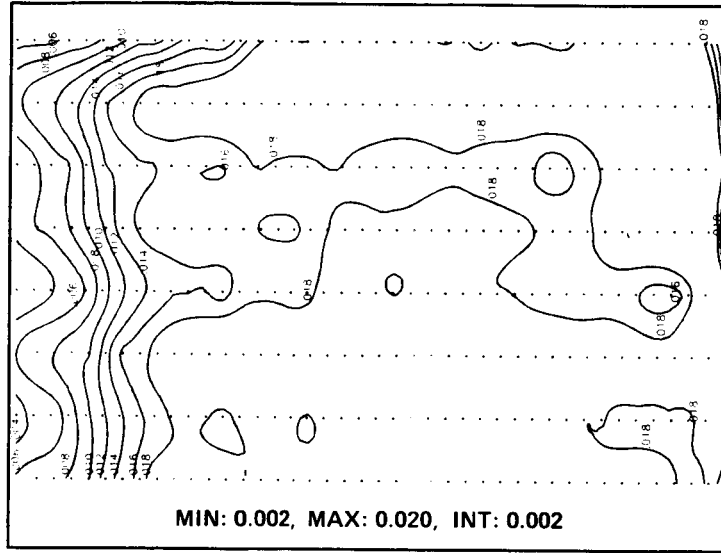
LOOKING UPSTREAM   **5.9% AIR EXCHANGE**

MIN: 0.08, MAX: 0.24, INT: 0.02
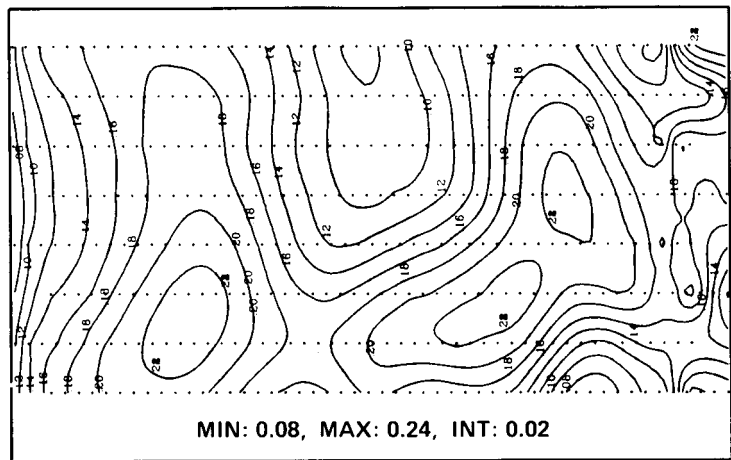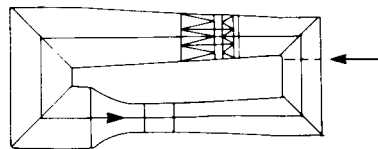
10.1% AIR EXCHANGE

LOCATION OF CROSS-STREAM SURVEYS

Figure 28.- Contours of the dynamic pressure coefficient downstream of the air-exchange inlet across the north end of the 1/50th-scale model of the 40 by 80. (a) 5.9% air exchange. b) 10.1% air exchange.

5.9% AIR EXCHANGE LOOKING UPSTREAM

COURTYARD SIDEWALL

C_p RANGE
MIN : 0.08
MAX : 0.26
INT : 0.02

VANE SET 2

FLOW DIRECTION

SURVEY LOCATION

LOCATION OF TRAILING EDGE OF AIR EXCHANGE DOOR

CEILING

FLOOR

10.1% AIR EXCHANGE LOOKING UPSTREAM

COURTYARD SIDEWALL

C_p RANGE
MIN : 0.08
MAX : 0.24
INT : 0.02

VANE SET 2

FLOW DIRECTION

SURVEY LOCATION

LOCATION OF TRAILING EDGE OF AIR EXCHANGE DOOR

CEILING

FLOOR
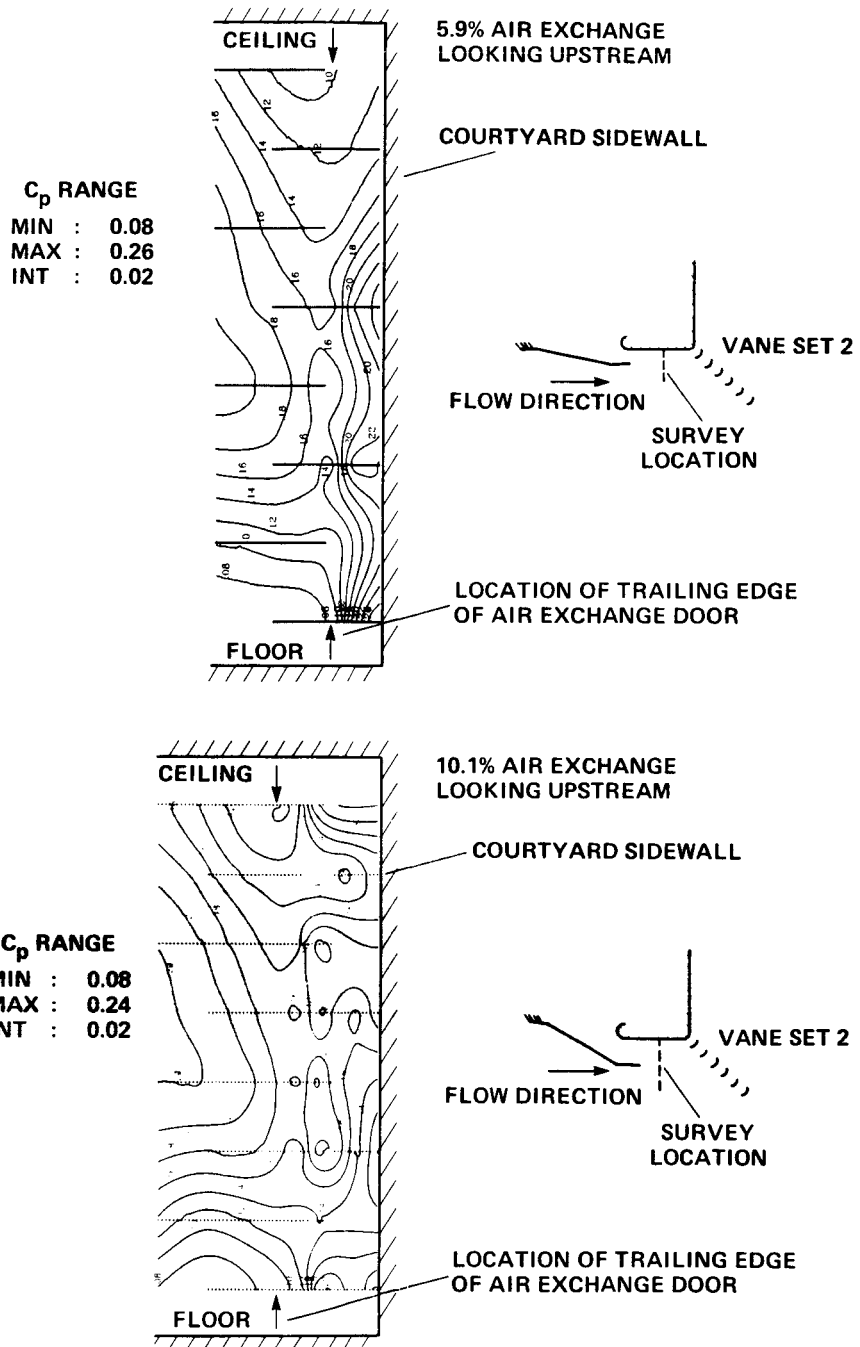
Figure 29.- Contours of the dynamic pressure coefficient downstream of the air-exchange door of the 1/50th-scale model of the 40 by 80. (a) 5.9% air exchange, looking upstream. (b) 10.1% air exchange, looking upstream.
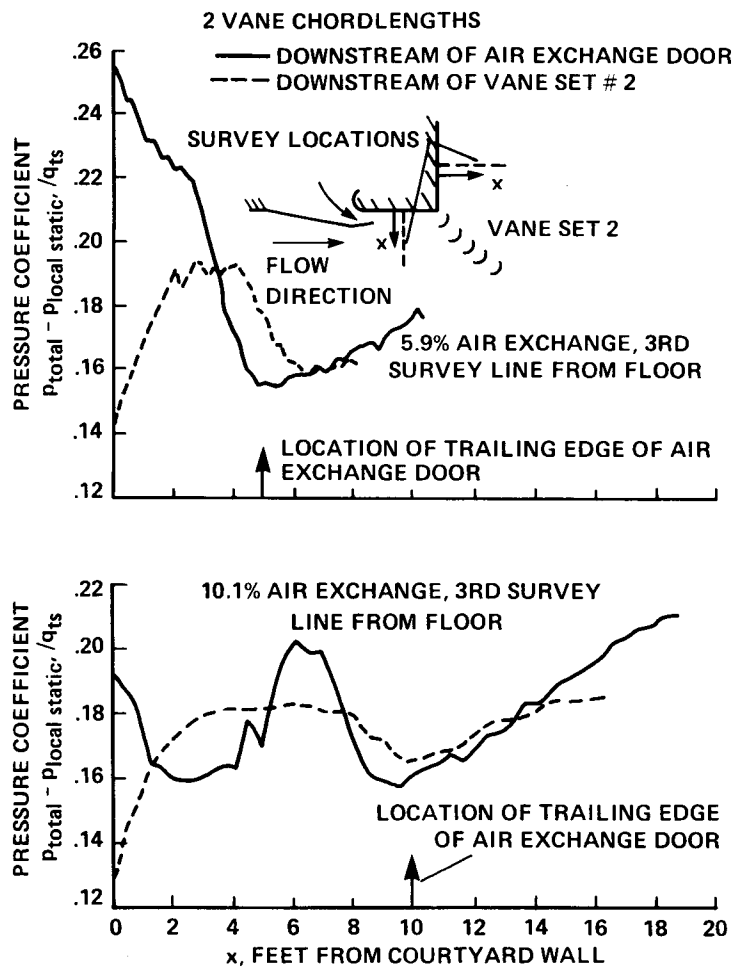
Figure 30.- Dynamic pressure coefficient profiles near courtyard wall of north end of the 1/50th-scale model of the 40 by 80. (a) 5.9% air exchange, 5th survey line from floor. (b) 10.1% air exchange, 5th survey line from floor.
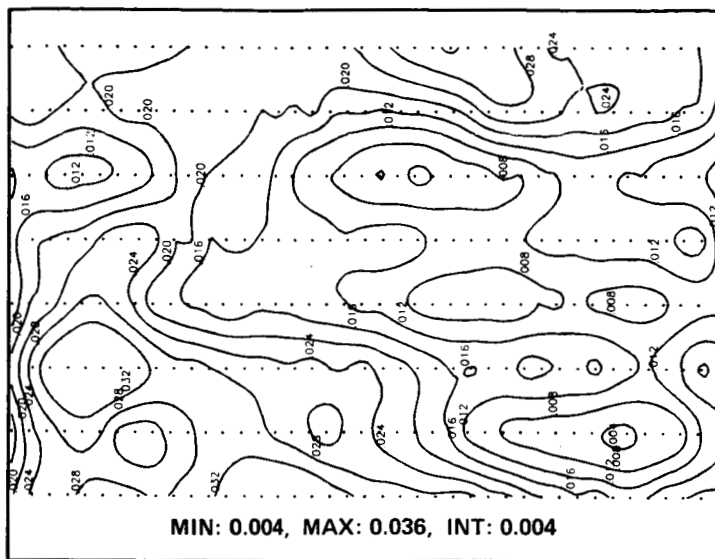
MIN: 0.004, MAX: 0.036, INT: 0.004

LOOKING UPSTREAM   5.9% AIR EXCHANGE

MIN: 0.004, MAX: 0.040, INT: 0.004
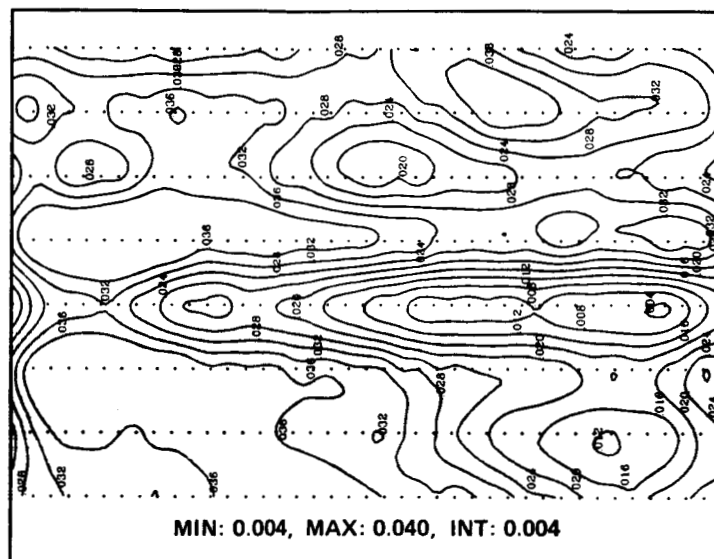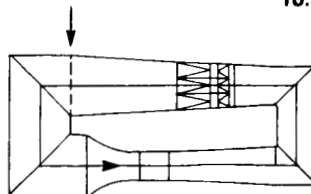
10.1% AIR EXCHANGE

LOCATION OF CROSS-STREAM SURVEYS

Figure 31.- Contours of the dynamic pressure coefficient across the downstream end of the fan diffuser of the 1/50th-scale model of the 40 by 80. (a) 5.9% air exchange. (b) 10.1% air exchange.

41

MIN: 0.002, MAX: 0.020, INT: 0.002

LOOKING UPSTREAM   **0% AIR EXCHANGE**

MIN: 0.002, MAX: 0.020, INT: 0.002

5.9% AIR EXCHANGE

LOCATION OF CROSS-STREAM SURVEYS

Figure 32.- Contours of the dynamic pressure coefficient across the south end of the 1/50th-scale model of the 40 by 80. (a) 0% air exchange. (b) 5.9% air exchange.

42

MIN: 0.002, MAX: 0.020, INT: 0.002

LOOKING UPSTREAM   **10.1% AIR EXCHANGE**
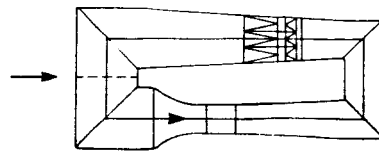
LOCATION OF CROSS-STREAM SURVEY

Figure 32.- Concluded. (c) 10.1% air exchange.
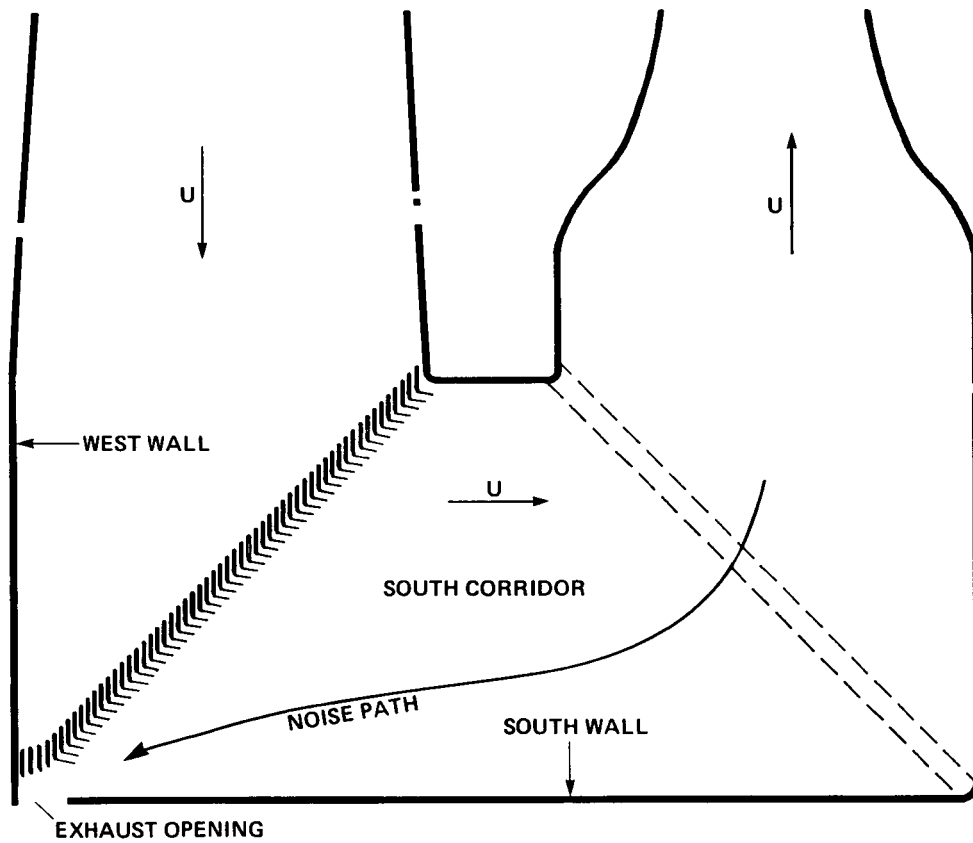
Figure 33.- Plan view of as-built south end of the 40 by 80 (40 by 80 mode).
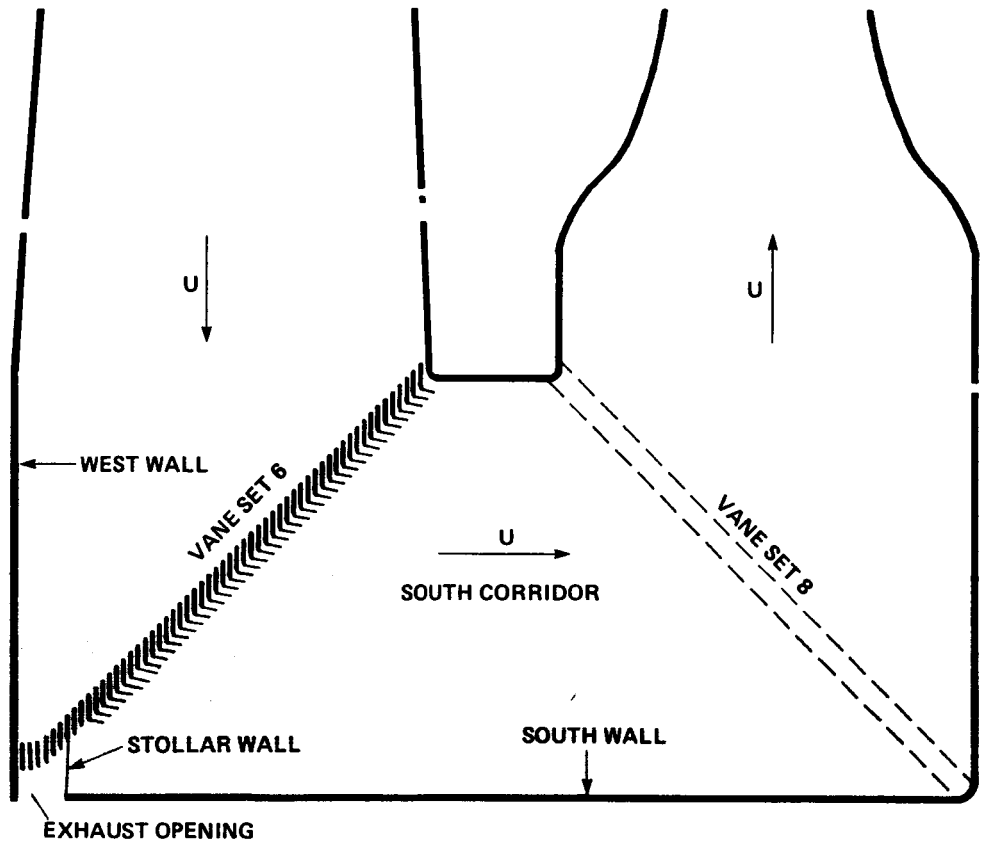
Figure 34.- Plan view of south end of the 40 by 80 with Stollar wall installed (40 by 80 mode).
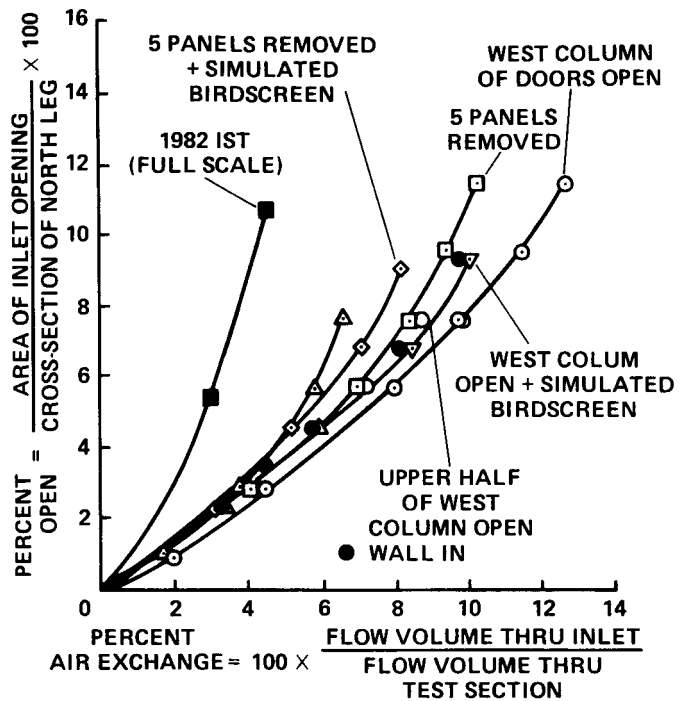
Figure 35.- Opening of courtyard inlet required to obtain a given air-exchange rate for several exhaust configurations. (Open symbols denote 1/50th-scale data.)
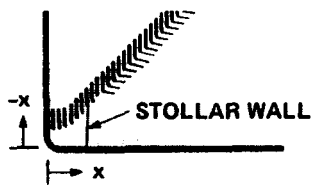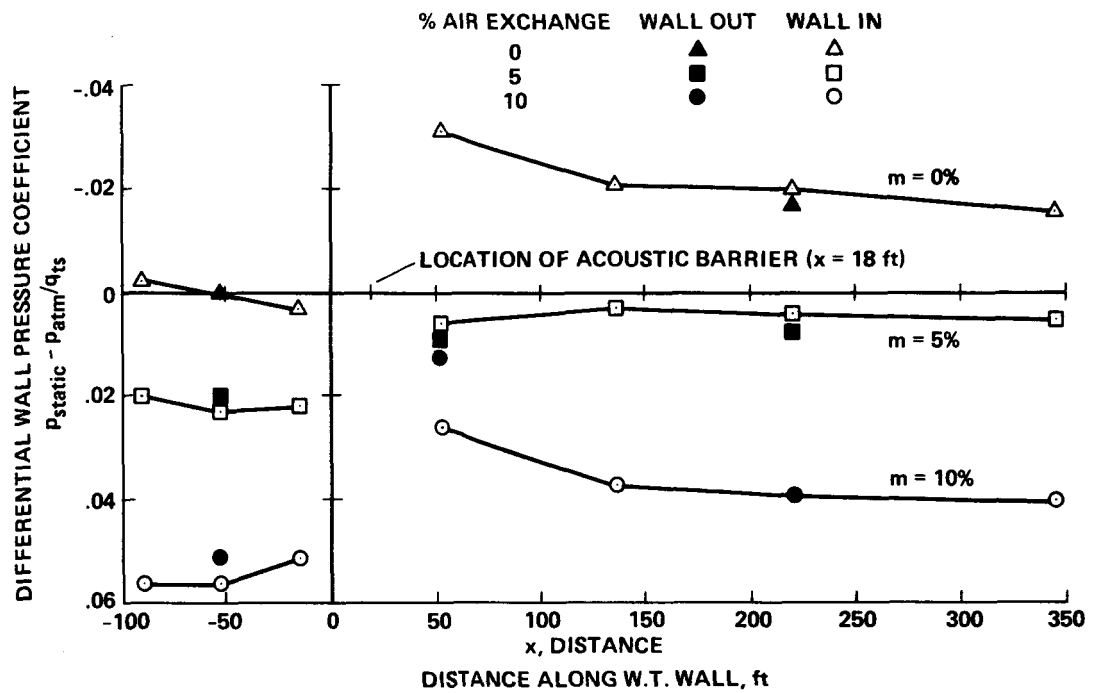
Figure 36.- Effect of air-exchange rate on south-end pressures of the 1/50th-scale model of the 40 by 80 (acoustic barrier is in and two flaps adjacent to barrier removed).
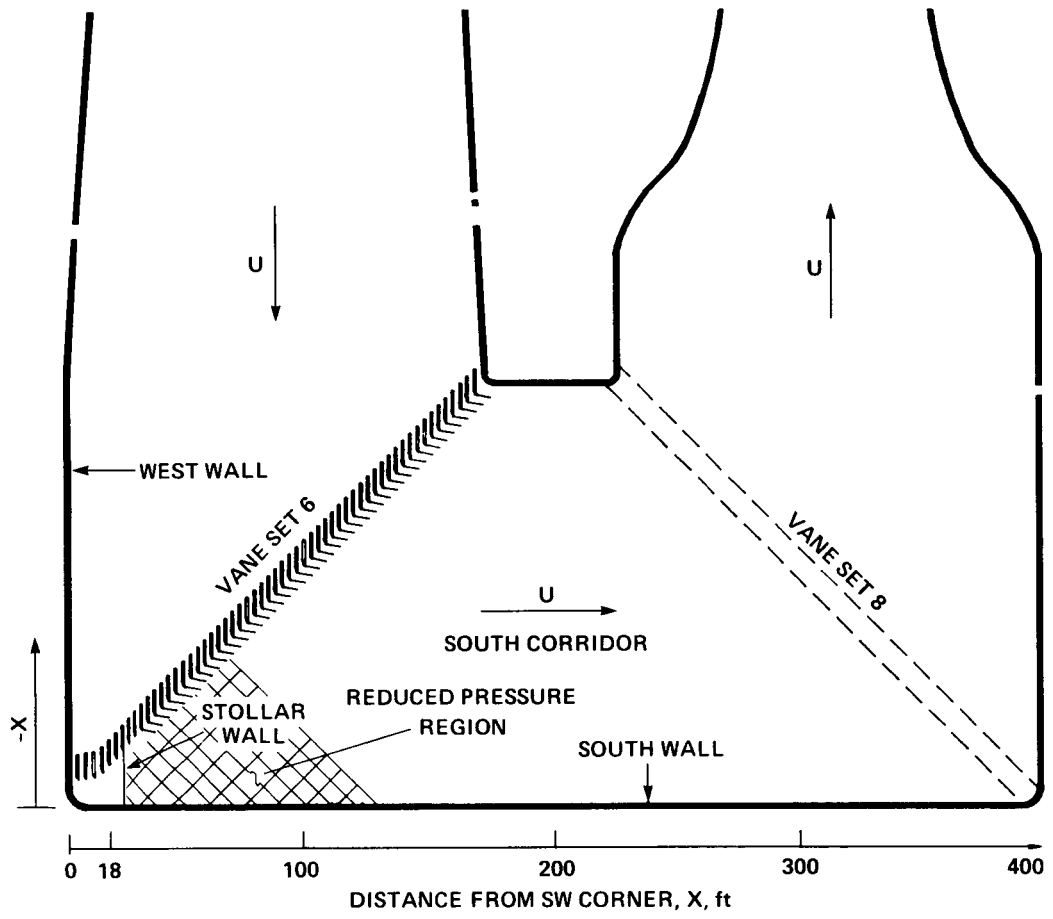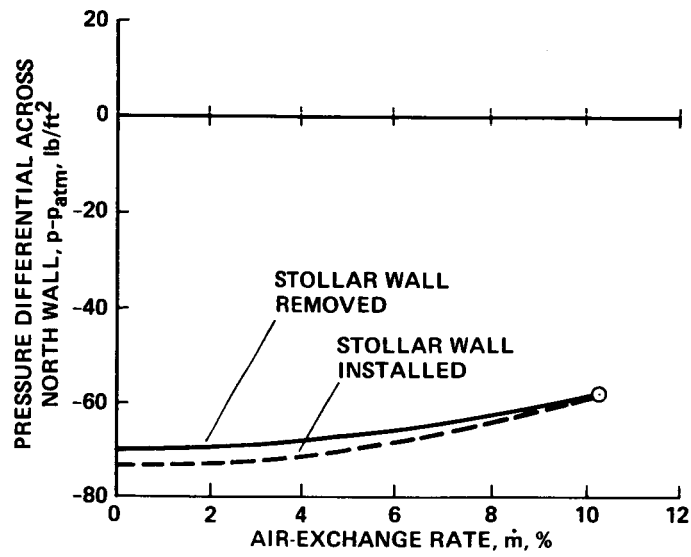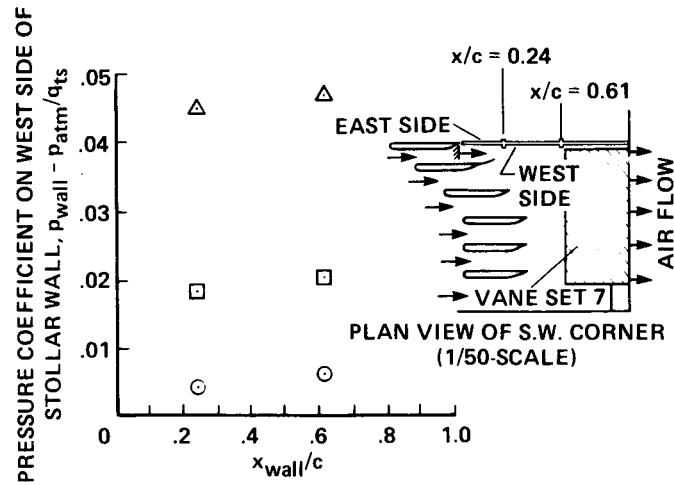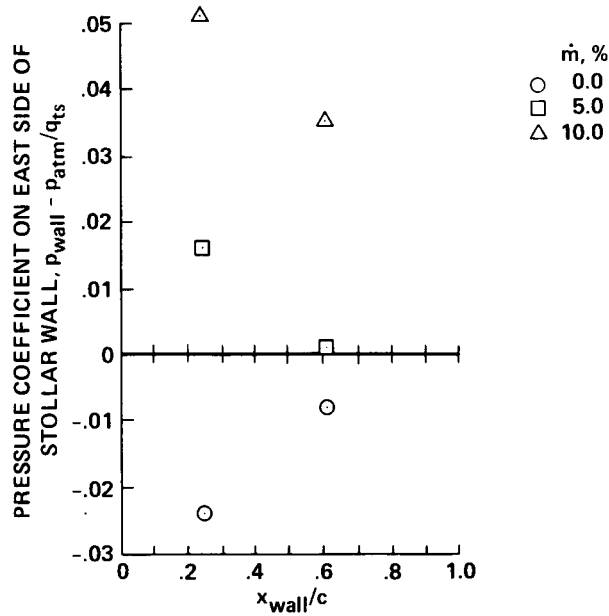
Figure 37.- South corridor, 40 by 80.
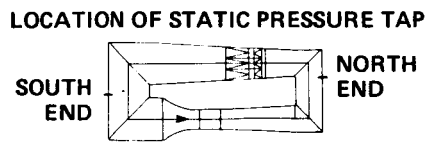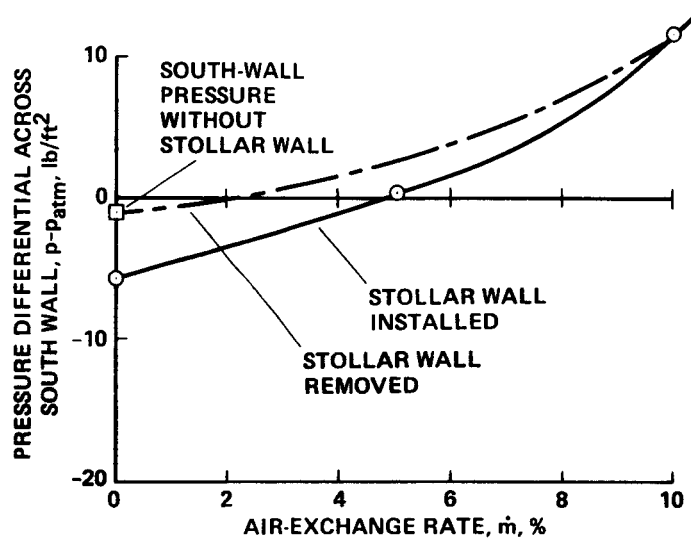
Figure 38.- Effect of air-exchange rate on wall pressure. (a) North end. (b) South end.
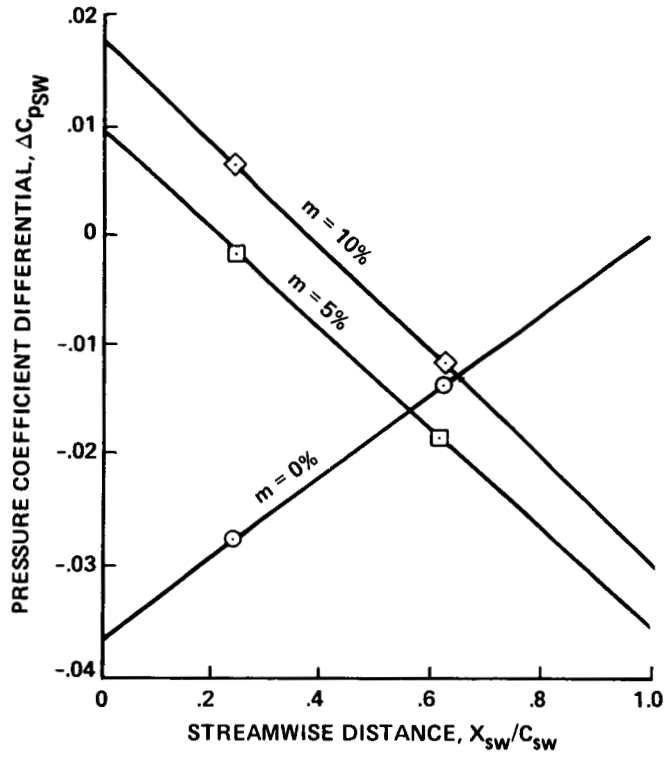
Figure 39.- Pressure on Stollar wass versus air-exchange rate. (a) Pressure on west side of Stollar wall versus air-exchange rate. (b) Pressure on east side of Stollar wall versus air-exchange rate.

50

$$\Delta C_{P_{SW}} = \left\{ \begin{array}{l} \text{STATIC PRESSURE} \\ \text{ON EAST SIDE} \\ \text{OF ACOUSTIC BARRIER} \end{array} \right. \begin{array}{l} \text{STATIC PRESSURE} \\ - \text{ON WEST SIDE} \\ \text{OF ACOUSTIC BARRIER} \end{array}$$

over q_{ts}

$$= \left\{ \begin{array}{l} + \text{LOAD} \equiv \text{EAST TO WEST} \\ - \text{LOAD} \equiv \text{WEST TO EAST} \end{array} \right.$$

$(\Delta C_{P_{SW}})^{*}$ MAX TO WEST = 0.0175

$(\Delta C_{P_{SW}})^{**}$ MAX TO EAST = -0.0372

DIRECTION	MAX. LOAD ON BARRIER	
	$|\Delta C_P|_{SW}$	#/ft^2
EAST TO WEST m = 10%	0.0175	4.58
WEST TO EAST m = 0%	0.0372	9.83

MEASUREMENT UNCERTAINTY $\sim \pm 0.006\ C_{P_{ts}}$

$\sim \pm 2\ \text{lb/ft}^2$

Figure 40.- Effect of air-exchange rate on pressure across Stollar wall ($q_{ts} = 262\ \text{lb/ft}^2$).
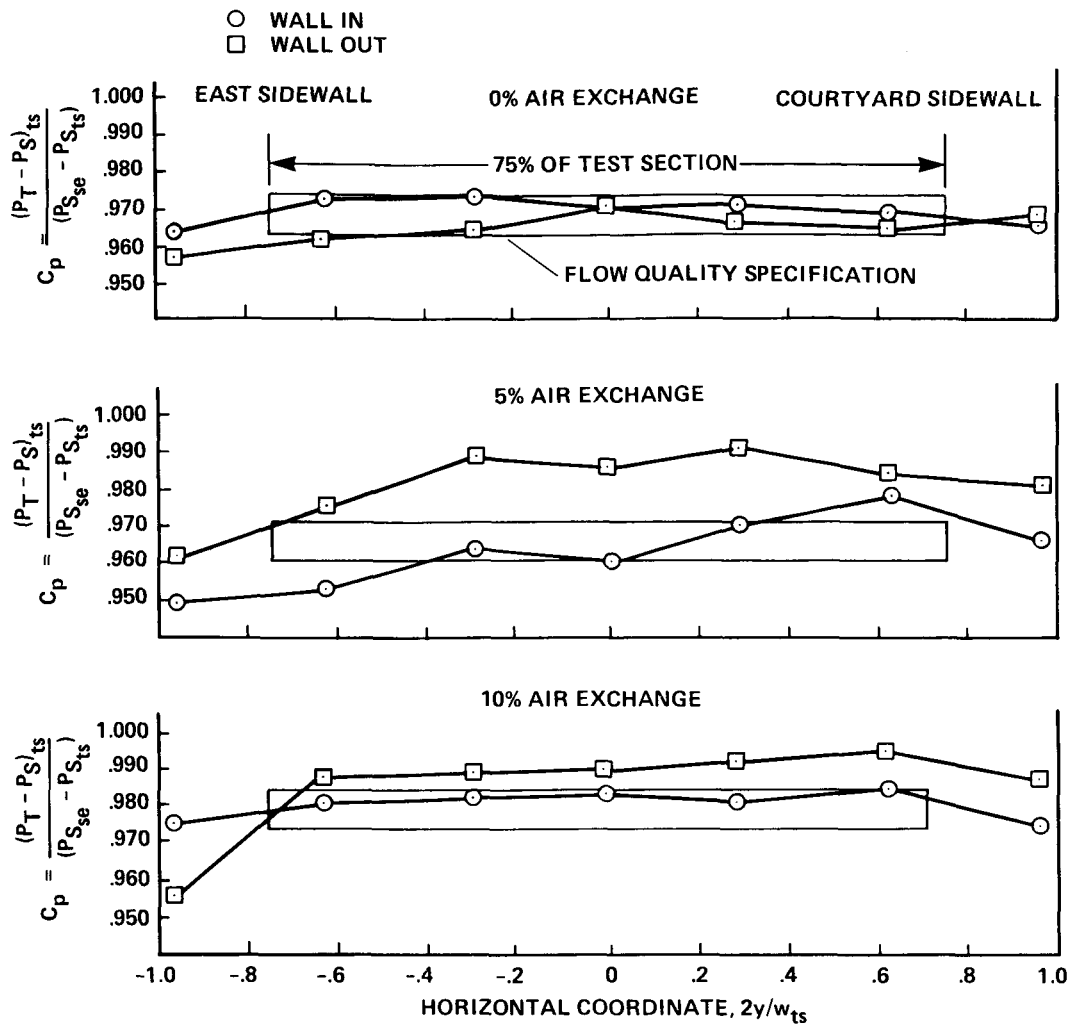
Figure 41.- Effect of acoustic barrier on the lateral distribution of the dynamic pressure coefficient in test section of the 1/50th-scale model of the 40 by 80.
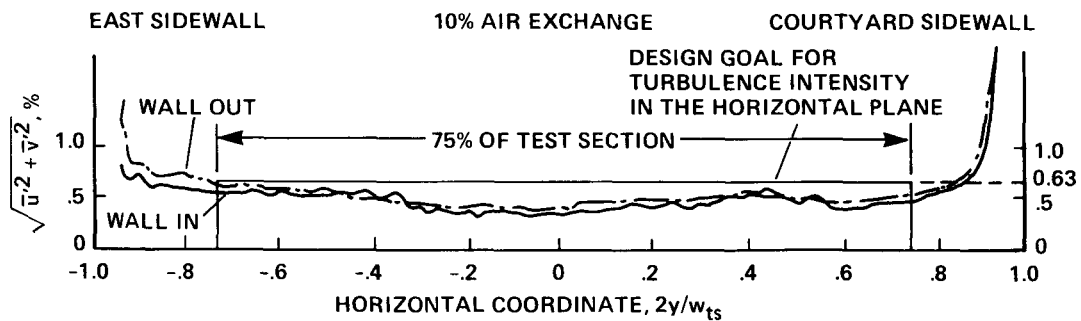

Figure 42.- Effect of acoustic barrier on lateral distribution of turbulence intensity in the test section of the 1/50th-scale model of the 40 by 80.

NASA
National Aeronautics and Space Administration

Report Documentation Page

1. Report No. NASA TM 88336	2. Government Accession No.	3. Recipient's Catalog No.

4. Title and Subtitle
Aerodynamic Characteristics of the Modified 40- by 80-Foot Wind Tunnel as Measured in a 1/50th-Scale Model

5. Report Date
August 1987

6. Performing Organization Code

7. Author(s)
Brian E. Smith and Tim Naumowicz (Robinson Engineering, San Carlos, CA)

8. Performing Organization Report No.
A-86329

10. Work Unit No.
505-60-21

9. Performing Organization Name and Address
Ames Research Center
Moffett Field, CA 94035

11. Contract or Grant No.

13. Type of Report and Period Covered
Technical Memorandum

12. Sponsoring Agency Name and Address
National Aeronautics and Space Administration
Washington, DC 20546

14. Sponsoring Agency Code

16. Abstract

The aerodynamic characteristics of the 40- by 80-Foot Wind Tunnel at Ames Research Center were measured by using a 1/50th-scale model of the full-scale facility. The model was configured to closely simulate the features of the full-scale facility when it becomes operational in 1986. The items measured include the aerodynamic effects due to changes in the total-pressure-loss characteristics of the intake and exhaust openings of the air-exchange system, total-pressure distributions in the flow field at locations around the wind tunnel circuit, the locations of the maximum total-pressure contours, and the aerodynamic changes caused by the installation of the acoustic barrier in the southwest corner of the wind tunnel. The model tests reveal the changes in the aerodynamic performance of the 1986 version of the 40- by 80-Foot Wind Tunnel compared with the performance of the 1982 configuration.

17. Key Words (Suggested by Author(s))
Wind tunnel
Pressure distribution
Air exchange
Flow-field survey

18. Distribution Statement
Unclassified-Unlimited

Subject Category - 02

19. Security Classif. (of this report) Unclassified	20. Security Classif. (of this page) Unclassified	21. No. of pages 56	22. Price A04